J Nonlinear Sci (2013) 23:39–95
DOI 10.1007/s00332-012-9139-0

Journal of Nonlinear Science

Rise and Fall of Periodic Patterns for a Generalized Klausmeier–Gray–Scott Model

Sjors van der Stelt · Arjen Doelman · Geertje Hek · Jens D.M. Rademacher

Received: 4 December 2011 / Accepted: 22 June 2012 / Published online: 19 July 2012

Abstract In this paper we introduce a conceptual model for vegetation patterns that generalizes the Klausmeier model for semi-arid ecosystems on a sloped terrain (Klausmeier in Science 284:1826–1828, 1999). Our model not only incorporates downhill flow, but also linear or nonlinear diffusion for the water component.

To relate the model to observations and simulations in ecology, we first consider the onset of pattern formation through a Turing or a Turing–Hopf bifurcation. We perform a Ginzburg–Landau analysis to study the weakly nonlinear evolution of small

Communicated by Alan R. Champneys.

S. van der Stelt (✉) · G. Hek
Korteweg-de Vries Instituut, Universiteit van Amsterdam, P.O. Box 94248, 1090 GE Amsterdam, The Netherlands
e-mail: stelt@cwi.nl

G. Hek
e-mail: G.M.Hek@uva.nl

S. van der Stelt · J.D.M. Rademacher
Centrum Wiskunde en Informatica (CWI), Science Park 123, 1098 XG Amsterdam, The Netherlands

J.D.M. Rademacher
e-mail: rademach@cwi.nl

A. Doelman
Mathematisch Instituut, Universiteit Leiden, P.O. Box 9512, 2300 RA Leiden, The Netherlands
e-mail: doelman@math.leidenuniv.nl

G. Hek
Institut International de Lancy, Avenue Eugène Lance 24, 1218 Geneva, Switzerland

amplitude patterns and we show that the Turing/Turing–Hopf bifurcation is supercritical under realistic circumstances.

In the second part we numerically construct Busse balloons to further follow the family of stable spatially periodic (vegetation) patterns. We find that destabilization (and thus desertification) can be caused by three different mechanisms: fold, Hopf and sideband instability, and show that the Hopf instability can no longer occur when the gradient of the domain is above a certain threshold. We encounter a number of intriguing phenomena, such as a 'Hopf dance' and a fine structure of sideband instabilities. Finally, we conclude that there exists no decisive qualitative difference between the Busse balloons for the model with standard diffusion and the Busse balloons for the model with nonlinear diffusion.

Keywords Reaction–diffusion systems · Nonlinear diffusion · Bifurcation · Periodic patterns · Continuation · Ginzburg–Landau · Busse balloons

Mathematics Subject Classification 35K57 · 35B32 · 35B36 · 35Q56 · 34L16

1 Introduction

In semi-arid ecosystems, a striking example of pattern-formation is found. After the first discovery in the 1950s in sub-Saharan Africa by aerial photographs (Macfadyan 1950a, 1950b), this type of patterned vegetation has been subject of various studies. As semi-arid ecosystems often mark the landscape between deserts or dry steppes on the one side and greener ecosystems on the other side, analysis of their vegetated patterns may help to understand desertification processes. This is a major reason why ecologists have performed much fieldwork (cf. Elwell and Stocking 1976; Kelly and Walker 1976; Rietkerk et al. 2000; Kéfi et al. 2007b), modeling and simulations (cf. Thiery et al. 1995; Levefer and Lejeune 1997; van de Koppel et al. 2002; Rietkerk et al. 2004; Kéfi et al. 2007a) in the past decades.

A major goal has been to examine whether and how the presence of patterned vegetation indicates proximity to a so-called catastrophic shift—a sudden drop to desert state. The current work is inspired by bifurcation-type diagrams in Rietkerk et al. (2002, 2004) which indicate that the catastrophic shifts most likely occur for long-wavelength patterns with very localized vegetation. In mathematical terms, these would be pulse patterns with narrow, high peaks and large interpulse regions. This suggests that the catastrophic shifts may be related to (homoclinic bifurcations of) single-pulse patterns. See Doelman et al. (1997) for examples for the Gray–Scott equation.

Various simulations of a three-component reaction–diffusion equation modeling plant-water-interactions (Rietkerk et al. 2002) show existence of stable large-amplitude vegetation patterns for parameter choices close to a Turing–Hopf bifurcation. As such bifurcations give rise to *small*-amplitude patterns, the question arises how these large-amplitude patterns are related to the bifurcation. One possibility would be that the Turing–Hopf bifurcation is subcritical, so that patterns that arise at the bifurcation are unstable and would hence not be observed (in simulations). Other, larger amplitude, stable patterns could bifurcate from these initially unstable patterns and could be the ones found in simulations.

The simplest model used to describe semi-arid ecosystems is the Klausmeier model (Klausmeier 1999). In the present paper, we extend this model and analyze whether it would allow for subcritical Turing–Hopf bifurcations. This is, however, only our first step: the core of the paper concerns our study for which parameter conditions (stable) vegetated patterns exist as solutions to the model. The emergence of small amplitude periodic patterns ('Ginzburg–Landau analysis') and the stability region of general periodic patterns in parameter space ('Busse balloons') play a major role in our analysis. Moreover, to our knowledge, we present the first Ginzburg–Landau analysis and Busse-balloon computations for systems with nonlinear diffusion. In particular, our results significantly add to the very sparse case studies of the structure of Busse balloons, particularly in reaction–diffusion-type models.

1.1 Origin of the Model

Semi-arid ecosystems are ecosystems with an annual precipitation of 250–500 mm, which are typically found at the edge of deserts. At the other side, greener ecosystems such as grass savannas, montane forests and temperate broadleaf forests are found. After the first report of patterned vegetation in sub-Saharan Africa (Macfadyan 1950a, 1950b), such patterns have been reported in many semi-arid ecosystems in Africa, the Americas and Australia. They are estimated to cover about 30 % of the emerging surface of the earth. The composition of the vegetation varies wildly from one ecosystem to another and can comprise grass, scrubs, bushes or trees (Levefer and Lejeune 1997; Macfadyan 1950b). Also, the occurrence of these patterns is not specific to the type of soil (Levefer and Lejeune 1997). Therefore, attempts have been made to describe them with models that focus on other possible mechanisms, most notably plant–plant interactions (Levefer and Lejeune 1997) or plant–water interactions (Klausmeier 1999; HilleRisLambers et al. 2001; Rietkerk et al. 2002).

Early attempts to formulate a model along these lines use cellular automata (Thiery et al. 1995) or mean field models (Levefer and Lejeune 1997). In 1999, C.A. Klausmeier was the first to model the dynamic interplay between surface water and vegetation by a reaction–(advection–)diffusion system (Klausmeier 1999). He introduced a conceptual 2-component model to describe patterns in semi-arid ecosystems, the components representing water u and biomass/vegetation v. In unscaled form, the model he introduced reads

$$\begin{cases} u_t = k_0 u_x + k_1 - k_2 u - k_3 k_5 u v^2; \\ v_t = d_v v_{xx} - k_4 v + k_5 u v^2, \end{cases} \tag{1.1}$$

where $u(x,t), v(x,t) : \mathbb{R} \times \mathbb{R}_+ \to \mathbb{R}$ and $k_i \geq 0$, $i = 0, \ldots, 5$, $d_v \geq 0$. The flow of water u_t is assumed to be governed by advection caused by the slope of the area, modeled by $k_0 u_x$, a constant precipitation rate k_1, an evaporation rate that is linear in the amount of water $-k_2 u$, and an infiltration feedback, modeled by $-k_3 k_5 u v^2$. It assumes that the change of biomass is controlled by a diffusive spread of biomass, modeled by a diffusion term $d_v v_{xx}$, a linear natural death rate $-k_4 v$, and the infiltration feedback $k_5 u v^2$, which has a positive effect on the vegetation. Since the spread

of biomass occurs on a much slower time scale than the advection of surface water, it is natural to assume $d_v \ll k_0$. The equilibrium $v = 0$, $u = k_1/k_2$ corresponds to the desert. Though the model is simplistic in nature, it is able to capture essential features of semi-arid ecosystems, such as the emergence of patterned vegetation.

Klausmeier's original model (Klausmeier 1999) assumed two-dimensional spatial variation in x and y of both biomass v and water u. In this article, we focus on its one-dimensional dynamics by assuming a constant variation in the direction of the spatial y-variable. We also assume that both u and v vary on an infinite domain $\mathbb{R}$ instead of a bounded domain $[0, L]$ with $L \in (0, \infty)$. This assumption is natural, since the scale of the observed patterns is very small compared to the size of the domain (cf. Deblauwe et al. 2008; HilleRisLambers et al. 2001; Klausmeier 1999; Macfadyan 1950a, 1950b; Rietkerk et al. 2002 and the references therein).

Klausmeier's model (1.1) assumes the existence of some slope or gradient that lets the water flow downhill and the growing vegetation migrate uphill. However, patterns have been observed as well in semi-arid ecosystems without a slope (Macfadyan 1950a, 1950b; White 1970). In order to model the spread of water on a terrain without a specific preference for the direction in which the water flows, we extend the model (1.1) by adding a term $d_u(u^\gamma)_{xx}$ for a priori possibly nonlinear diffusion. We thus obtain

$$\begin{cases} u_t = d_u \left(u^\gamma\right)_{xx} + k_0 u_x + k_1 - k_2 u - k_3 k_5 u v^2; \\ v_t = d_v v_{xx} - k_4 v + k_5 u v^2, \end{cases} \tag{1.2}$$

where it is assumed that $\gamma \geq 1$. Since the spread of biomass occurs on a much slower scale than the (nonlinear) diffusion of water, it is again natural to assume $0 < d_v \ll d_u$. For ecosystems without a slope, we set $k_0 = 0$. In this article we mainly focus on $\gamma = 1$ or $\gamma = 2$. The choice $\gamma = 1$ simplifies the spread of water to linear diffusion, whereas $\gamma = 2$ is based on a less (over)simplified way to model the motion of water—see Remarks 1 and 2. Of course the present generalization of Klausmeier's model still is a conceptual model—only the basic mechanisms are taken into account and these are modeled in a highly simplified fashion.

In order to reduce the number of parameters, we rescale the equations. We set

$$U = \frac{k_2}{k_1} u; \qquad V = \frac{k_2 k_3}{k_1} v, \tag{1.3}$$

and further

$$T = \frac{k_1^2 k_5}{k_2^2 k_3} t; \qquad X = \left[d_u \frac{k_3}{k_5} \left(\frac{k_1}{k_2} \right)^{\gamma - 3} \right]^{-\frac{1}{2}} x \tag{1.4}$$

to obtain

$$\begin{cases} U_t = U_{xx}^\gamma + C U_x + A(1 - U) - U V^2, \\ V_t = \delta^{2\sigma} V_{xx} - B V + U V^2, \end{cases} \tag{1.5}$$

with

$$A = k_2 \frac{k_2^2 k_3}{k_1^2 k_5}; \qquad B = k_4 \frac{k_2^2 k_3}{k_1^2 k_5}; \qquad C = k_0 \frac{k_2^2 k_3}{k_1^2 k_5} \left[d_u \frac{k_3}{k_5} \left(\frac{k_1}{k_2} \right)^{\gamma - 3} \right]^{-\frac{1}{2}}$$

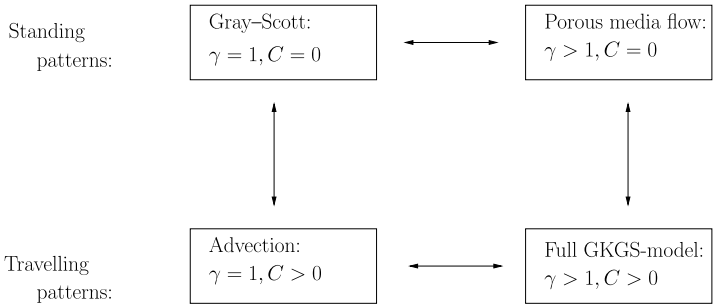

Fig. 1 A schematic picture of the GKGS-model. On the *top line*, the models without advection ($C = 0$) are depicted. These models generate symmetric Turing patterns that are modulated according to a real GLE. On the *bottom line*, the models with a nontrivial advection rate $C > 0$ are depicted. For these models, the appearance of the traveling periodic patterns is described by a complex GLE. (See Sect. 2.4)

and

$$\delta^{2\sigma} = \frac{d_v}{d_u}\left(\frac{k_2}{k_1}\right)^{\gamma-1} \quad (\sigma > 0).$$

Here $0 < \delta \ll 1$, since $0 < d_v \ll d_u$. Notice that there is a redundancy in the introduction of $\delta > 0$ in $\delta^{2\sigma}$, which will be clarified in Sect. 2. The system parameters A, B, C, and γ are chosen according to the characteristics of the ecosystem under study. In particular, ecosystems without a slope are by setting $C = 0$ and ecosystems on a sloped terrain are modeled by setting $C \neq 0$. We may view C as a parameter that measures the rate of advection, A as a parameter that controls the precipitation and B as a parameter that describes the extinction rate of the biomass.

It is naturally to assume that C and B are constant and to vary A—as is also typically done in the Gray–Scott model (see Morgan et al. 2000). This change in A may cause desertification. Throughout this paper, we therefore consider A as our major parameter—see Remark 3. A priori, there is no reason to assume that the parameters A, B, and C are $\mathcal{O}(1)$ with respect to δ; in fact, the relative magnitudes of A, B, and C will play a crucial role in the upcoming analysis (see also Morgan et al. 2000).

The above rescaling is motivated by the fact that equation (1.5) reduces to the well-studied Gray–Scott model if we set $C = 0$ and $\gamma = 1$ (see Chen and Ward 2009; Doelman et al. 1997; Morgan et al. 2000 and the references therein). We refer to the equations in (1.5) as *the Generalized Klausmeier–Gray–Scott model* or, for short, GKGS-model. By either setting $\gamma = 1$ or $\gamma > 1$ and either $C = 0$ or $C > 0$, the GKGS-model comprises four types of equation. A schematic picture of the four classes of the GKGS-system is given in Fig. 1. Klausmeier's model (albeit in a different scaling than in Klausmeier (1999)) is derived if we set $d_u = 0$ or, somewhat artificially, $\gamma = 0$. However, his model can also be derived as a limit case for $C \to \infty$ in a proper scaling of the GKGS-model (see Sect. 2.6).

Remark 1 In the formulation of the Klausmeier model in Klausmeier (1999), the author does not explicitly distinguish between surface water, i.e. water on top of the soil, and soil water, water penetrated into the soil. In later, more extended models,

this distinction indeed has been made—see for instance Gilad et al. (2004), HilleRis-Lambers et al. (2001), Rietkerk et al. (2002) and the references therein. For both possible interpretations—$u(x,t)$ as surface water or as soil water in (1.2)—a linear diffusion term, i.e. $\gamma = 1$, for the spread of water is possible, but strongly simplified. In Gilad et al. (2004), it is deduced by a shallow water argument that for a thin layer of water on top of the soil, $u(x,t)$ diffuses in a nonlinear fashion (more precisely: the arguments in Gilad et al. (2004) imply that $\gamma = 2$ in (1.2)). Since the soil is in general a porous medium, flow of (soil) water through this medium naturally is of porous media type, i.e. of nonlinear diffusion type as in (1.2). Again, the most typical nonlinear value of γ is 2, although in principle other values of γ (≥ 1) are also possible—see for instance Fowler (1997). Note that the 'infiltration feedback' term $k_3 k_5 u v^2$ is modeled as a negative effect in (1.1): this is an (implicit) indication that $u(x,t)$ should be interpreted as surface water in Klausmeier (1999).

Remark 2 For $\gamma \neq 1$ system (1.2) turns from a standard, semilinear parabolic, reaction–diffusion system into a quasilinear one, which is mathematically much less convenient to handle. However, since the solutions we consider in this paper have uniformly positive u-values, we stay in the well-behaved parabolic regime. A suitable abstract framework of well-posedness and nonlinear semi-groups in quasi-linear problems that in principle covers equations of the type (1.2), (1.5) can be found, e.g., in Amann (1990), Kato (1975). Details will appear elsewhere (Siero and Rademacher 2012).

Remark 3 The expression for A depends on the rainfall parameter k_1 via $A \sim k_2^3/k_1^2$. At first sight, this may seem contradictory, since in the rescaled model (1.5) we argued that A acts as a parameter that measures the rainfall. Moreover, the appearance (and subsequent disappearance) of vegetation patterns is initiated by decreasing A, which at first sight seems to correspond to increasing the rainfall parameter k_1. However, we have seen that B in (1.5) is proportional to k_2^2/k_1^2. Thus, the assumption that B and k_j, $j = 3,4,5$, are constant, implies that $k_1 \sim k_2$, and therefore $A \sim \frac{k_2^3}{k_1^2} \sim \frac{k_1^3}{k_1^2} = k_1$. Hence, we see that A is directly proportional to the rainfall k_1 (under the assumption that B is constant). It should also be noted that exactly the same analysis as is done in this paper by varying A in (1.5) (and keeping all other parameters fixed), can also be performed directly on the unscaled equation (1.2), in which one can then—for instance—only vary the rainfall parameter k_1.

1.2 Outline of the Analysis and Conclusions

The GKGS-model (1.5) has the same three spatially homogeneous background states as the Gray–Scott model for $A > 4B^2$ (in fact, the homogeneous dynamics of both systems is identical):

$$\begin{aligned} &U_0 = 1, \qquad V_0 = 0, \\ &U_\pm = \frac{1}{2A}\left(A \mp \sqrt{A^2 - 4AB^2}\right), \qquad V_\pm = \frac{1}{2B}\left(A \pm \sqrt{A^2 - 4AB^2}\right). \end{aligned} \tag{1.6}$$

The state $(U_0, V_0) = (1, 0)$ represents the desert (since $V_0 \equiv 0$). At $A_{\mathrm{sn}} = 4B^2$, the equilibria (U_+, V_+) and (U_-, V_-) collapse and disappear in a fold, or saddle node bifurcation. Hence, for $A < A_{\mathrm{sn}}$, the desert $(U_0, V_0) = (1, 0)$ is the only background state, while for $A > A_{\mathrm{sn}}$, we have three background states, of which two represent homogeneously vegetated states.

This paper is a first step in the analysis of GKGS model for vegetation patterns. In Sects. 2.1–2.4, we describe analytically the emergence of spatially periodic vegetation patterns by a Turing or a Turing–Hopf bifurcation of the stationary state (U_+, V_+) by deriving a (complex) Ginzburg–Landau Equation (GLE) for each of the four classes in Fig. 1. The derivation of the GLE as modulation equation for Turing patterns in reaction–diffusion equations is a well-known, but certainly nontrivial procedure (see for instance Morgan et al. 2000 for the Turing bifurcation in the Gray–Scott model). Here we show that this procedure can also be applied to reaction–diffusion–advection equations with nonlinear diffusion—to our knowledge this has not been shown before in the literature (see Sect. 2.4).

We derive that the Turing–Hopf bifurcation is supercritical for ecologically relevant parameter combinations in each of the four classes, regardless the values we choose for B and C. This answers one of our initial questions: for realistic parameter values the simple Klausmeier model cannot account for a subcritical Turing bifurcation, not even in an extended form with (nonlinear) diffusion. It appears that for $\gamma = 1$ (normal diffusion), the Turing(–Hopf) bifurcation is always supercritical, regardless the value of the advection rate C. For the Gray–Scott case $C = 0$, $\gamma = 1$, this was already known (Morgan et al. 2000). However, we find that the Turing(–Hopf) bifurcation becomes subcritical if $\gamma > \gamma_{ss} \approx 13$. Though it does not occur at a relevant parameter value for the ecology, this is an interesting mathematical observation: the nonlinearity of the diffusion is able to trigger a change from super- to subcriticality while a change of the advection rate C is not.

Related to the Ginzburg–Landau analysis, we have evaluated the associated Benjamin–Feir–Newell criterion (Aranson and Kramer 2002 and Sect. 2.4). Our analysis shows that there always exists a band of stable periodic patterns near a Turing(–Hopf) bifurcation for ecologically relevant parameter combinations. Note that this is quite remarkable, given the dimensions of the parameter space.

We also show that the Klausmeier model appears as a limit case of the GKGS-model for large C and derive an explicit Ginzburg–Landau equation for the Klausmeier model that shows the Turing–Hopf bifurcation of the Klausmeier system to be supercritical as well.

The Ginzburg–Landau analysis is weakly nonlinear in the sense that it can only be applied if the GKGS-system is close to the critical parameter value A_* for A at which a Turing–Hopf instability takes place, that is, if $|A - A_*| \ll 1$. In the second part of this paper (Sect. 3), we extend the analysis to more general parameter values A. By expanding recently developed numerical techniques for the continuation of instabilities of periodic patterns (Rademacher et al. 2007), we present a rather complete picture of all instabilities that spatially periodic patterns of our reaction–advection–diffusion models can undergo for all relevant ecological parameters (cf. Rademacher and Scheel 2007). In particular, we present complete regions in (A, κ)-space (here κ is the wavenumber of the periodic vegetation pattern) where stable periodic patterns exist. Such regions are called Busse balloons (see Sect. 3 for a more precise

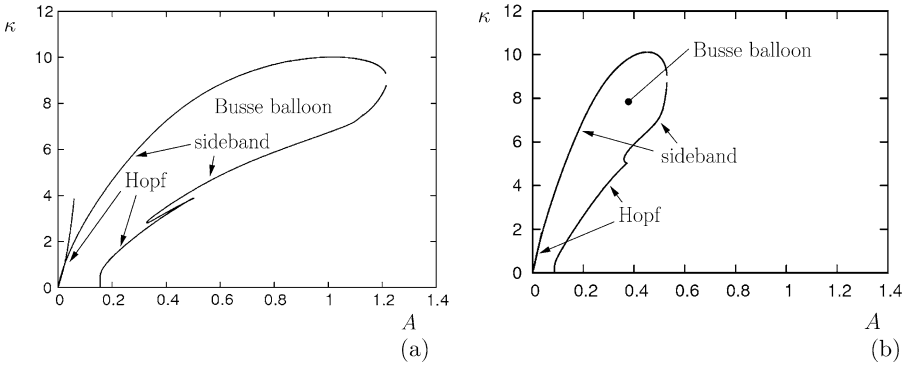

Fig. 2 (**a**) Busse balloon for $B = C = 0.2$ and $\gamma = 1$. (**b**) Busse balloon for $B = C = 0.2$ and $\gamma = 2$. Notice that the scale of the axes in both pictures is the same. In both cases, the boundary consists of a branch of sideband instabilities that is crossed by a curve of Hopf instabilities both on the *left* as well as on the *right*. Somewhat surprisingly, the only difference between the Busse balloons for $\gamma = 1$ (**a**) and $\gamma = 2$ (**b**) is of a quantitative nature

definition)—see Fig. 2 for some first examples. In each of the four classes in Fig. 1, we construct a Busse balloon for a number of relevant parameter combinations, giving a complete overview of all the instabilities that periodic patterns can undergo as a function of A (given that the other parameters are fixed).

We find that periodic patterns destabilize in three different types of instability: fold (only if $C = 0$), Hopf and sideband. (Note that the fold cannot be a robust destabilization mechanism in non-reversible systems (Rademacher and Scheel 2007).) Somewhat surprisingly, we find that the characteristics of the Busse balloon do, contrary to the type of Turing bifurcation, depend heavily on C and not on γ (for its most realistic values 1 and 2). See Figs. 2(a) and (b). We mention our most important results. Firstly, we show the existence of the so-called Hopf-dance for $C = 0$, both for the case of linear as well as for nonlinear diffusion; note that the Hopf dance has been elaborately described in Doelman et al. (2012). If $C \neq 0$, the two intertwining branches of Hopf instabilities are replaced by a 'curtain' of Hopf instabilities. Our second main observation is that this Hopf curve moves out of the Busse balloon in an intriguing—and certainly non-understood fashion. Thirdly, we find that—independent of the type of destabilization (Hopf/sideband), the homoclinic ($\kappa = 0$) pattern always is the last one to become unstable. This corroborates Ni's conjecture (Doelman et al. 2012; Ni 1998) and generalizes it significantly to nonreversible systems with nonlinear diffusion. Fourthly, for relatively small values of C there exists a rich and unexplained fine structure for the sideband instabilities (mostly in the unstable region). Finally, once more we note explicitly the remarkable fact that the differences between a Busse balloon for $\gamma = 1$ and a Busse balloon for $\gamma = 2$ are only quantitative: the step from linear diffusion ($\gamma = 1$) to nonlinear diffusion with $\gamma = 2$ triggers no qualitative changes in the structure of the Busse balloon.

Remark 4 The mathematical approach to equations of Klausmeier–Gray–Scott type of the present work is related to several papers in the literature. First of all, in Sherratt (2005, 2010), Sherratt and Lord (2007) various aspects of the 'classical' Klausmeier

model—for instance, the linear stability analysis of its 'trivial patterns'—are studied. However, the weakly nonlinear stability analysis of the onset of pattern formation in the Klausmeier model as presented in section 2.6 is new in the literature on this model. In Kealy and Wollkind (2012), a nonlinear stability analysis in a Klausmeier-type model is presented. In fact, in Kealy and Wollkind (2012) the advection term of the Klausmeier model is replaced by a linear diffusion term. In our terminology, this means that the Gray–Scott model is considered in that paper. In this sense, Kealy and Wollkind (2012) strongly relates to Morgan et al. (2000). Finally, in Satnoianu et al. (2001), Satnoianu and Menzinger (2000) spatially periodic patterns in Gray–Scott type equations with an additional advection term are considered: a situation that is similar to the lower-left side case of Fig. 1 ($\gamma = 1$, $C > 0$). Again, the linear mechanism leading to—in our terminology—Turing–Hopf patterns is studied. However, it is not followed by a weakly nonlinear Ginzburg–Landau analysis.

2 The Rise of Patterns

Before we embark upon a study of the onset of patterns in the GKGS-system, let us introduce some terminology that will be used throughout the article. Reaction–diffusion–advection systems like (1.5) naturally allow for spatially periodic solutions. These spatially periodic patterns or *wave trains* are solutions $u(x,t)$ that can be written as $u(x,t) = u_{\mathrm{per}}(\kappa x + \Omega t)$ and that satisfy $u_{\mathrm{per}}(\xi) = u_{\mathrm{per}}(\xi + 2\pi)$. Here κ is called the *(nonlinear) wavenumber* and Ω is the *(nonlinear) frequency*. A wave train is called a *background state* or *stationary state* when both its wavenumber and frequency are zero, i.e., when $u(x,t) \equiv u_{\mathrm{per}}(0)$ for all $x \in \mathbb{R}$, $t \in [0,\infty)$. It is called a *Turing pattern* if its frequency is zero, i.e., when $u(x,t) = u_{\mathrm{per}}(\kappa x)$ for all $x \in \mathbb{R}$, $t \in [0,\infty)$: Turing patterns have standing profiles. A generic wave train has $\kappa \neq 0$ and $\Omega \neq 0$ and will therefore have a traveling profile with velocity Ω/κ.

In this section we derive critical parameter values for which the stationary state (U_+, V_+) 1.6 undergoes a Turing–Hopf instability and derive a leading order form for $0 < \delta \ll 1$ of the GKGS-model (1.5) near the Turing–Hopf bifurcation. The stationary state (U_-, V_-) is always unstable, as can be readily checked. Subsequently, we derive a Ginzburg–Landau equation for the slowly modulating amplitude of the periodic pattern that appears at the Turing–Hopf instability. In order to employ a leading order analysis in (1.5) for $0 < \delta \ll 1$, we follow Morgan et al. (2000) and scale the parameters by

$$A = a\delta^{\alpha}, \qquad B = b\delta^{\beta} \quad \text{and} \quad C = c\delta^{\nu}, \tag{2.1}$$

with $\alpha, \beta > 0, \nu \in \mathbb{R}$ and $a, b, c = \mathcal{O}(1)$ with respect to δ. The background state (U_+, V_+) can then be written out to leading order in δ as

$$(U_+, V_+) = \left(\frac{b^2}{a}\delta^{2\beta-\alpha}, \frac{a}{b}\delta^{\alpha-\beta}\right) + \text{h.o.t.} \tag{2.2}$$

We notice that the two states $(U_\pm, V_\pm)$ only exist if $A \geq A_{\mathrm{sn}} = 4B^2$, or equivalently, $a \geq 4b^2\delta^{2\beta-\alpha}$. Since δ is assumed asymptotically small, boundedness of a yields the condition

$$2\beta - \alpha \geq 0, \tag{2.3}$$

with equality allowed only if $a \geq 4b^2$.

2.1 The Turing and Turing–Hopf Instabilities

The linearized GKGS-system about the stationary state $u_+ = (U_+, V_+)$ can be written abstractly as

$$u_t = \mathcal{D}u_{xx} + \mathcal{C}u_x + \partial_u F(u_+; A, B)u =: \mathcal{L}[\partial_x]u, \tag{2.4}$$

with $u = (U, V)$, $F(U, V; A, B) := (A(1-U) - UV^2, -BV + UV^2)$, $\mathcal{D}$ the matrix defined by $\mathcal{D} = \mathrm{diag}(\gamma U_+^{\gamma-1}, \delta^{2\sigma})$ and $\mathcal{C}$ the matrix defined by $\mathcal{C} = \mathrm{diag}(C, 0)$.

We consider the spectrum $\mathrm{spec}\,\mathcal{L}[\partial_x]$ of the operator $\mathcal{L}[\partial_x]$ defined in (2.4) and define the matrix $\mathcal{M}$ by

$$\mathcal{M}(a, c, \mathrm{i}k) := \begin{pmatrix} -\gamma(U_+)^{\gamma-1}k^2 + \mathrm{i}c\delta^\nu k - V_+^2 - \delta^\alpha a & -2b\delta^\beta \\ V_+^2 & -\delta^{2\sigma}k^2 + \delta^\beta b \end{pmatrix}. \tag{2.5}$$

Notice that $\mathcal{M}(a, c, \mathrm{i}k) = \mathcal{L}[\mathrm{i}k]$. As can be seen by computing the Fourier transform of (2.4) w.r.t. x, a complex number $\lambda \in \mathbb{C}$ belongs to the L^2-spectrum of $\mathcal{L}[\partial_x]$ if there exists a $k \in \mathbb{R}$ such that

$$d(\lambda, \mathrm{i}k) := \det\big[\mathcal{M}(a, c, \mathrm{i}k) - \lambda\big] = 0. \tag{2.6}$$

Equation (2.6) is called the (linear) *dispersion relation* of (1.5) about (U_+, V_+). We refer to k as the (linear) wavenumber. It is associated to a Fourier mode of the perturbation of the background state (U_+, V_+). Recall that the nonlinear wavenumber κ is the wavenumber of the bifurcating wave train itself, it should thus not be confused with the linear wavenumber k of perturbations to the wave train. We can now make a basic definition, analogous to Scheel (2003).

Definition 1 $\mathcal{L}[\partial_x]$ is called *marginally stable* with critical Fourier mode $u_0 \mathrm{e}^{\mathrm{i}k_* x}$ associated to the unique critical eigenmode $\mathrm{i}\omega_*$, up to complex conjugation, if:

1. $d(\mathrm{i}\omega_*, \mathrm{i}k_*) = 0$.
2. $d(\mathrm{i}\omega_*, \mathrm{i}k) \neq 0$ for all $k \neq \pm k_*$.
3. $d(\lambda, \mathrm{i}k) \neq 0$ for all $k \in \mathbb{R}$ and all $\lambda \in \mathbb{C}$ with $\lambda \neq \mathrm{i}\omega_*$ and $\mathrm{Re}\,\lambda \geq 0$.

Two possible spectral configurations of the background state (U_+, V_+) at marginal stability are depicted in Fig. 3. Definition 1 does not provide an explicit scheme to determine marginal stability. In practice, one uses the following necessary (though a priori not sufficient) conditions to derive marginal stability of $\mathcal{L}$ with respect to eigenfunction $U_0 \mathrm{e}^{\mathrm{i}k_* x}$ and eigenvalue $\mathrm{i}\omega_*$:

$$\mathrm{Re}\,\lambda|_{k=k_*} = 0 \quad \text{and} \tag{2.7a}$$

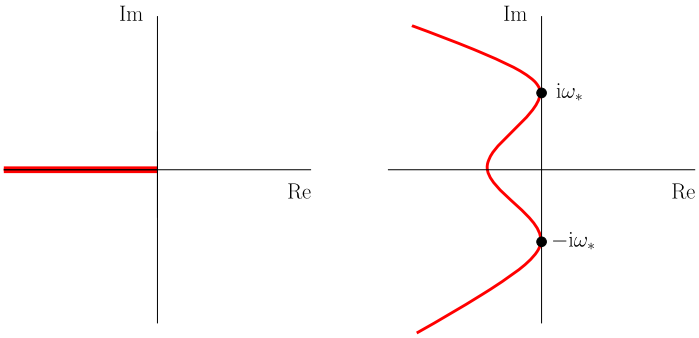

Fig. 3 The *thick lines* denote possible typical configurations of a spatially periodic perturbation of the background state at marginal stability in the complex λ-plane. On the *left*, the spectrum near the origin is real, as is typical for the (reversible) GKGS-model with $C = 0$. On the *right*, $C \neq 0$

$$\left.\frac{\partial \operatorname{Re}\lambda}{\partial k}\right|_{k=k_*} = 0. \tag{2.7b}$$

We call the instability a *Turing–Hopf* instability if the wavenumber and its associated frequency of the eigenmode at marginal stability are nonzero, $k_* \neq 0$, $\omega_* \neq 0$, and we call the instability a *Turing* instability if the frequency of the eigenfunction at marginal stability is zero, i.e., $\omega_* = 0$ and $k_* \neq 0$ (see Fig. 3). It will be confirmed in Sects. 2.2 and 2.3 that (U_+, V_+) undergoes a Turing instability to Turing patterns if $C = 0$ and a Turing–Hopf instability to generic wave trains if $C \neq 0$.

2.2 Critical Parameters for the GKGS-Model with $C = 0$

First we derive the critical parameter a_* and critical wavenumber k_* at which the stationary state (U_+, V_+) undergoes a Turing instability for the GKGS-model with $C = 0$. For $C = 0$, the dispersion relation (2.6) can be written as

$$\begin{aligned} d(\lambda, \mathrm{i}k) &= \det\big[\mathcal{M}(a, 0, \mathrm{i}k) - \lambda I\big] \\ &= \lambda^2 - \operatorname{tr}\mathcal{M}(a, 0, \mathrm{i}k)\lambda + \det\mathcal{M}(a, 0, \mathrm{i}k). \end{aligned} \tag{2.8}$$

If Definition 1 for marginal stability holds, then the trace $\operatorname{tr}\mathcal{M}(a, \mathrm{i}k) = \lambda_- + \lambda_+$ cannot be positive. Substitution of the leading order formulation for V_+ yields

$$-\gamma\delta^{(2\beta-\alpha)(\gamma-1)}\left(\frac{b^2}{a}\right)^{\gamma-1}k^2 - \frac{a^2}{b^2}\delta^{2(\alpha-\beta)} - \delta^\alpha a - \delta^{2\sigma}k^2 + \delta^\beta b \leq 0. \tag{2.9}$$

Recall $a, b > 0$. For this inequality to hold, also at $k = 0$, it is needed that either $2(\alpha - \beta) \leq \beta$ or $\alpha \leq \beta$. Since the weakest of these conditions suffices, we impose

$$2\alpha \leq 3\beta. \tag{2.10}$$

Notice that this condition is stricter than (2.3). We are now in the position to formulate the following proposition concerning marginal stability.

Proposition 1 *Let* $C = 0$, $\gamma \geq 1$, *and* $0 < \delta \ll 1$, *and define* $g := 3 - 2\sqrt{2}$. *The background state* (U_+, V_+) *of* (1.5) *is marginally stable for* σ, $a = a_*$, *and* $k = k_*$ *satisfying*

$$\begin{aligned} (2\gamma+1)\beta - (\gamma+1)\alpha &= 2\sigma \\ k_*^2 &= \frac{1}{2}(1-g)b\delta^{-2\gamma\beta+(\gamma+1)\alpha} \\ a_*^{\gamma+1} &= g\gamma b^{2\gamma+1}, \end{aligned} \tag{2.11}$$

to leading order in δ.

Notice that we recover Proposition 3.1 of Morgan et al. (2000) for the Gray–Scott model if we set $\gamma = 1$.

Proof We first show that, as expected from the reversible symmetry for $C = 0$, an instability always occurs through the origin so that it suffices to consider the simple case $\lambda = \omega_* = 0$ at $k = k_*$.

Suppose that $d(\mathrm{i}\omega, \mathrm{i}k) = 0$ and note that $\mathcal{M}(a, 0, \mathrm{i}k)$ is real. According to (2.8)

$$\operatorname{Im} d(\mathrm{i}\omega, \mathrm{i}k) = \omega \operatorname{tr} \mathcal{M}(a, 0, \mathrm{i}k) = 0,$$

so that either $\omega = 0$ (which means $\lambda = 0$) or $\operatorname{tr}\mathcal{M} = 0$. The latter implies

$$\operatorname{tr} \mathcal{M}(a, 0, \mathrm{i}k) = -\left(\gamma (U_+)^{\gamma-1} + \delta^{2\sigma}\right)k^2 + \operatorname{tr}\mathcal{M}(a, 0, 0) = 0,$$

which has real roots k if and only if $\operatorname{tr}\mathcal{M}(a, 0, 0) > 0$, which is clearly not the case by (2.9).

Therefore it suffices to consider $\lambda = 0$ and prove that there exist a_* and k_* such that

$$\det \mathcal{M}(a_*, 0, \mathrm{i}k_*) = 0, \tag{2.12a}$$

$$\frac{\partial}{\partial k} \det \mathcal{M}(a_*, 0, \mathrm{i}k_*) = 0. \tag{2.12b}$$

From (2.12b) we get

$$k_*^2 = -\frac{\delta^{2\sigma} V_+^2 + \delta^{2\sigma+\alpha} a_* - \gamma \delta^{\beta} U_+^{\gamma-1} b}{2\gamma \delta^{2\sigma} U_+^{\gamma-1}}. \tag{2.13}$$

From this expression, substitution of $\gamma\delta^{2\sigma} U_+^{\gamma-1}$ in (2.12a) yields

$$k_*^2 = \frac{-2\delta^{\beta} b(V_+^2 - \delta^{\alpha} a_*)}{\delta^{2\sigma} V_+^2 + \delta^{2\sigma+\alpha} a_* - \gamma\delta^{\beta} U_+^{\gamma-1} b}. \tag{2.14}$$

Before we solve a_* from the combination of (2.13) and (2.14) we first determine its magnitude. Since k_*^2 in (2.13) is positive, one obtains, by using the leading order expression (2.2),

$$\frac{a_*^2}{b^2}\delta^{2(\alpha-\beta+\sigma)} + a_*\delta^{2\sigma+\alpha} - \gamma b\left(\frac{b^2}{a_*}\right)^{\gamma-1}\delta^{\beta+(2\beta-\alpha)(\gamma-1)} < 0. \tag{2.15}$$

It follows from (2.10) that $2(\alpha-\beta+\sigma) < 2\sigma+\alpha$, which means that condition (2.15) would be satisfied if $\beta + (2\beta-\alpha)(\gamma-1) \leq 2(\alpha-\beta+\sigma)$. Using (2.2) and (2.10), we deduce from (2.13) that k_*^2 is $\mathcal{O}(\delta^{\beta-2\sigma})$, and from (2.14) that k_*^2 is $\mathcal{O}(\delta^{2(\alpha-\beta)-(2\beta-\alpha)(\gamma-1)})$. Hence, we find a condition on the magnitude of the parameters at the Turing instability,

$$(2\gamma+1)\beta - (\gamma+1)\alpha = 2\sigma. \tag{2.16}$$

By substituting this in condition (2.15), we get

$$a_*^{\gamma+1} < \gamma b^{2\gamma+1}.$$

We can now consider the leading order expressions of (2.13) and (2.14), and conclude

$$\left(\frac{a_*^2}{b^3} - \gamma\left(\frac{b^2}{a_*}\right)^{\gamma-1}\right)^2 = 4\gamma\frac{a_*^2}{b^3}\left(\frac{b^2}{a_*}\right)^{\gamma-1}.$$

Solving this for a_* gives two solutions of which only one satisfies condition $a_*^{\gamma+1} < \gamma b^{2\gamma+1}$, hence

$$a_*^{\gamma+1} = g\gamma b^{2\gamma+1},$$

which also yields the leading order expression for k_*^2.

Since the spectral curves $\lambda_\pm(k^2)$ are solutions of the quadratic equation in λ (2.8), it is straightforward to show that $d(0,k_*)$ indeed satisfies Definition 1, i.e., that $\mathcal{L}$ is marginally stable. □

2.3 Critical Parameters for the GKGS-Model

Before we can study the critical parameters at which the (irreversible) Turing–Hopf instability occurs for $C \neq 0$, we first need to determine the (critical) scaling of C, that is, the critical value of the exponent ν (2.1). If C is too small (i.e., ν too large), it will only have a higher order impact on the analysis of the previous section. If C is very large, it will have a major impact on the linear stability. The critical scaling of C is determined by the value of ν at which the influence of C becomes of leading order in the linear stability analysis (this ν is a 'significant degeneration', cf. Eckhaus 1979). Therefore, we use the scalings obtained in Proposition 1 in $\mathcal{M}(a,c,\mathrm{i}k)$. Write $k = \delta^{\frac{1}{2}(\gamma+1)\alpha-\gamma\beta}\hat{k}$ (so that $\hat{k}_c = \mathcal{O}(1)$). The scalings for A, B, and C in (2.1) imply that we have, to leading order in δ,

$$\mathcal{M}(a,c,\mathrm{i}k) = \begin{pmatrix} \delta^{2\alpha-2\beta}[-\Gamma\hat{k}^2 - \frac{a^2}{b^2} + \mathrm{i}c\delta^{\nu-\frac{1}{2}(3-\gamma)\alpha-(\gamma-2)\beta}\hat{k}] & \delta^{\beta}[-2b] \\ \delta^{2\alpha-2\beta}[\frac{a^2}{b^2}] & \delta^{\beta}[-\hat{k}^2+b] \end{pmatrix}, \tag{2.17}$$

where we have introduced $\Gamma = \Gamma(\gamma, a) := \gamma(\frac{b^2}{a})^{\gamma-1}$. Hence, it follows that the critical scaling of ν is given by

$$\nu = \frac{1}{2}(3-\gamma)\alpha + (\gamma-2)\beta. \tag{2.18}$$

For this ν, the dispersion relation is determined by

$$\det\begin{pmatrix} \delta^{2\alpha-2\beta}[-\Gamma\hat{k}^2 - \frac{a^2}{b^2} + \mathrm{i}c\hat{k} - \delta^{3\beta-2\alpha}\hat{\lambda}] & \delta^{\beta}[-2b] \\ \delta^{2\alpha-2\beta}[\frac{a^2}{b^2}] & \delta^{\beta}[-\hat{k}^2 + b - \hat{\lambda}] \end{pmatrix} = 0, \tag{2.19}$$

where we have introduced $\hat{\lambda}$ by $\lambda = \delta^{\beta}\hat{\lambda}$.

It follows from (2.10) that the term with $\hat{\lambda}$ in the upper left entry of (2.19) is not of leading order. Hence, we conclude that at leading order in δ, and by dropping hats on $\hat{k}$ and $\hat{\lambda}$, the appearance of the Turing–Hopf instability is governed by the simplified dispersion relation

$$\det \mathcal{M}_{\lambda}(a, c, \mathrm{i}k) = 0, \tag{2.20}$$

with $\mathcal{M}_{\lambda}(a, c, \mathrm{i}k)$ defined as follows:

$$\mathcal{M}_{\lambda}(a, c, \mathrm{i}k) := \begin{pmatrix} -\Gamma k^2 - \frac{a^2}{b^2} + \mathrm{i}ck & -2b \\ \frac{a^2}{b^2} & -k^2 + b - \lambda \end{pmatrix}. \tag{2.21}$$

If we define

$$F(k) := \Gamma k^2 + \frac{a^2}{b^2} \quad \text{and} \quad G(k) := k^2 - b, \tag{2.22}$$

it follows from (2.21) that the dispersion relation of the GKGS-system (1.5) is, to leading order in δ,

$$\begin{aligned} d(\lambda, \mathrm{i}k) &:= \lambda[F - \mathrm{i}ck] + \det \mathcal{M}_0(a, c, \mathrm{i}k) \\ &\equiv \lambda[F - \mathrm{i}ck] + \det \mathcal{M}_0(a, 0, \mathrm{i}k) - \mathrm{i}ckG = 0. \end{aligned} \tag{2.23}$$

Recall that (2.7a), (2.7b) determines two necessary conditions for marginal stability. Substituting (2.7a) in (2.23) gives, to leading order in δ,

$$\begin{aligned} \omega ck + \det \mathcal{M}_0(a, 0, \mathrm{i}k) = 0, \\ \omega F - ckG = 0, \end{aligned} \tag{2.24}$$

where $\omega = \omega_*$ is the critical frequency defined by $\lambda(k)|_{k=k_*} = \mathrm{i}\omega_*$ (see Definition 1). Differentiation of (2.23) with respect to k yields, after substitution of the conditions in (2.7a), (2.7b),

$$\begin{aligned} \frac{\partial \omega}{\partial k} ck + \omega c + \partial_k \det \mathcal{M}_0(a, 0, \mathrm{i}k) = 0, \\ \frac{\partial \omega}{\partial k} F + \omega F' - cG - ckG' = 0. \end{aligned} \tag{2.25}$$

From the second equations in (2.24) and (2.25) it now follows that

$$\omega = \frac{ckG}{F} \quad \text{and} \quad \frac{\partial \omega}{\partial k} = \frac{c}{F^2}\big[F\big(G + kG'\big) - kGF'\big]. \tag{2.26}$$

Note that unlike in the case $c = 0$, here we have $\lambda(k)|_{k=k_*} = \mathrm{i}\omega_* \neq 0$. Thus the destabilization that sets in at marginal stability indeed is of Turing–Hopf type if $c \neq 0$. The right equation in (2.26) gives the *group velocity* $c_{\mathrm{g}} := -\frac{\partial \omega}{\partial k}|_{k=k_*}$, which may be interpreted as the velocity with which wave packets with Fourier spectrum centered around the frequency k_* evolve.

The equations in (2.24) and (2.25) give

$$\begin{aligned} \det \mathcal{M}_0(a, 0, \mathrm{i}k) &= -\frac{c^2 k^2 G}{F}, \\ \partial_k \det \mathcal{M}_0(a, 0, \mathrm{i}k) &= -\frac{kc^2}{F^2}\big[F\big(2G + kG'\big) - kGF'\big]. \end{aligned} \tag{2.27}$$

These equations determine a_* and k_* of Definition 1.

Proposition 2 *Let $0 < \delta \ll 1$, $\tilde{k} = \delta^{-\frac{1}{2}(\gamma+1)\alpha+\beta\gamma} k$ and drop the tilde on $\tilde{k}$, and let $C = c\delta^{\frac{1}{2}(3-\gamma)\alpha+(\gamma-2)\beta} \neq 0$. Let, as before, $g = 3 - 2\sqrt{2}$. The stationary state (U_+, V_+) undergoes a Turing–Hopf instability at a uniquely defined critical parameter $a = a_*$ and critical wavenumber $k = k_*$ that satisfy*

$$a_*^{\gamma+1} \geq g\gamma b^{2\gamma+1} \quad \textit{and} \tag{2.28a}$$

$$k_*^2 < b. \tag{2.28b}$$

If $c = \frac{2}{3} b\Gamma$, the Turing–Hopf instability takes place at the explicit parameter values, to leading order in δ,

$$a_*^{\gamma+1} = \frac{1}{3}\gamma b^{2\gamma+1} \quad \textit{and} \quad k_*^2 = \frac{1}{3} b.$$

Moreover, for $c \gg 1$, we have, to leading order in c and δ,

$$a_*^{\gamma+3}(c) = \frac{g}{\gamma} b^{2\gamma+3} c^2 + \mathcal{O}(c) \quad \textit{and} \quad k_*^2(c) = \frac{1}{2}(1-g)b + \mathcal{O}(1/c). \tag{2.29}$$

Proof First we show that a Turing–Hopf instability occurs. We rewrite equations (2.27) by

$$K = k^2 \quad \text{and} \quad E = \frac{a^2}{b^2} \tag{2.30}$$

to obtain

$$\begin{aligned} \left(K^2 + K\left(\frac{E}{\Gamma} - b\right) + \frac{E}{\Gamma} b\right)\left(K + \frac{E}{\Gamma}\right) &= -\left(\frac{c}{\Gamma}\right)^2 K(K - b), \\ \left(2K + \frac{E}{\Gamma} - b\right)\left(K + \frac{E}{\Gamma}\right)^2 &= -\left(\frac{c}{\Gamma}\right)^2 \left(K^2 + 2\frac{E}{\Gamma} K - \frac{E}{\Gamma} b\right), \end{aligned}$$

and we further introduce X, ρ, and η by

$$K = bX, \qquad \frac{E}{\Gamma} = b\rho \quad \text{and} \quad \frac{c^2}{\Gamma^2} = b\eta. \tag{2.31}$$

Then the equations simplify to

$$\begin{aligned} \big(X^2 + X(\rho-1) + \rho\big)(X+\rho) &= -\eta X(X-1), \\ \big[(X+\rho)\big(2X + (\rho-1)\big)\big](X+\rho) &= -\eta\big(X^2 + 2\rho X - \rho\big). \end{aligned} \tag{2.32}$$

As a shorthand we introduce polynomials f, g, h, and j and write (2.32) in the obvious way as

$$f(X,\rho)(X+\rho) = -\eta g(X), \tag{2.33a}$$

$$h(X,\rho)(X+\rho) = -\eta j(X,\rho). \tag{2.33b}$$

We view these as functions of X and sometimes suppress the dependence on ρ. With the above rescalings of a and k, the problem of finding a parameter $a = a_* > 0$ with wavenumber $k = k_*$ such that (2.27) holds, has been reduced to the problem of finding a $\rho > 0$ and an $X \geq 0$ such that (2.33a), (2.33b) hold. We may assume $\eta \neq 0$ (since the case $c = 0$ is dealt with in Proposition 1. From this and from (2.33a), (2.33b) it follows that we search for $X \geq 0$ such that

$$j(X)f(X) = g(X)h(X). \tag{2.34}$$

We notice the following:

$$j(0)\cdot f(0) = -\rho\cdot\rho = -\rho^2 < 0 \quad \text{and} \quad j(1)\cdot f(1) = (1+\rho)\cdot 2\rho > 0$$

while

$$g(0)h(0) = g(1)h(1) = 0.$$

Hence it follows that for each $\rho \in \mathbb{R}$, there is a $X = X_*(\rho) \in (0,1)$ such that (2.34) holds.

If $g(X_*) \neq 0$, we can define

$$\eta(\rho) := -\frac{f(X_*(\rho),\rho)}{g(X_*(\rho))}\big(X_*(\rho) + \rho\big). \tag{2.35}$$

The triplet $\rho, X_*(\rho), \eta(\rho)$ is a solution for (2.33a), (2.33b).

We need to consider the case $g(X_*) = 0$ or $j(X_*) = 0$ separately. We have $g(X) = 0$ if and only if $X = 0$ or $X = 1$. However, if $X = 0$ or $X = 1$, the first equation of (2.32) contradicts the assumption that $\rho > 0$, so we find that the condition $g(X_*) \neq 0$ is never violated. On the other hand, if $j(X_*) = 0$, then, by (2.33b), it must hold that $X_* = \frac{1}{2}(1-\rho)$. Solving $j(\frac{1}{2}(1-\rho)) = 0$ gives $\rho = \frac{1}{3}$ and therefore $X_* = \frac{1}{3}$. Substituting these values for X and ρ in (2.33a), gives $\eta = \frac{2}{3}$. Hence, by rewriting to original parameters, we obtain the special case for which

$$a_*^{\gamma+1} = \frac{1}{3}\gamma b^{2\gamma+1}, \qquad k_*^2 = \frac{1}{3}b \quad \text{and} \quad c = \frac{2}{3}b\Gamma.$$

We have now proven that for each $\rho > 0$, there is a pair $X_*(\rho), \eta(\rho)$ that solves (2.33a), (2.33b). In order to complete the proof it remains to show that for each $\eta > 0$ (and thus for each $c \in \mathbb{R}$), there is a unique pair $X_*(\eta)$, $\rho(\eta)$ (or k_*, a_*) that solves (2.33a), (2.33b). This can be proved by showing that $\eta(\rho)$ as defined in (2.35), attains each value in $[0, \infty)$ and is an invertible map.

By (2.32) it is easy to see that $\eta(\rho) = 0$ if $\rho = g$. On the other hand, as we will prove below, η is unbounded as a function of ρ: $\eta \to \infty$ if $\rho \to \infty$ (which by (2.31) is $c \to \infty$). Also, the function $\eta(\rho)$ has no (vertical) asymptotes since we saw that $g(X_*) \neq 0$. Hence, $\eta(\rho)$ attains each value in $[0, \infty)$. It now suffices to show that $\eta = \eta(\rho)$ is injective. This can be derived by a tedious analysis of the polynomials in (2.32): for all η there is at most one pair (X, ρ) such that (2.32) holds. We omit the details.

Next we derive the estimates in (2.28a), (2.28b). The estimate in (2.28b) follows from the fact that $0 < X_* < 1$ and we have (2.30) and (2.31). We prove the estimate in (2.28a). From (2.31) it is clear that η does not allow for negative values. That is, by (2.35), and since $g(X) < 0$ for all $X \in (0, 1)$, we can only allow for those ρ for which $\operatorname{sign}(f) > 0$. It is straightforward to show that $f(X) > 0$ for all $X \in (0, 1)$ if $\rho > g$, and $f(X) < 0$ for all $X \in (0, 1)$ if $\rho < g$. Hence, if we rewrite the condition $\rho > g$ in terms of the original parameters, we obtain (2.28a):

$$a_*^{\gamma+1} \geq g\gamma b^{2\gamma+1}.$$

Finally, we analyze the case for asymptotically large values of η (or equivalently, asymptotically large values for c and derive equations (2.29)). Consider equation (2.32). Since X_* is bounded ($|X_*| < 1$), we must rescale ρ and we obtain

$$\mathcal{O}\big(\rho^2\big) = \mathcal{O}(\eta).$$

We therefore set $\eta = \tilde{\eta}\rho^2$, with $\rho \gg 1$, and expand (2.32):

$$\begin{aligned} X + 1 &= -\tilde{\eta} X(X-1) + \mathcal{O}(1/\rho), \\ 1 &= -\tilde{\eta}(2X-1) + \mathcal{O}(1/\rho). \end{aligned}$$

Solving this gives, to leading order,

$$X_* = \frac{1}{2}(1-g) + \mathcal{O}(1/\rho) \quad \text{and} \quad \tilde{\eta}_* = 3 + 2\sqrt{2} + \mathcal{O}(1/\rho).$$

Rescaling X_* back to k_* and $\tilde{\eta}_*$ back to a_* and c gives (2.29),

$$k_*^2 = \frac{1}{2}(1-g)b + \mathcal{O}(1/c) \quad \text{and} \quad a_*^{\gamma+3}(c) = \frac{g}{\gamma} b^{2\gamma+3} c^2 + \mathcal{O}(c). \qquad \square$$

2.4 Modulation Equations for the Rising Patterns

At the Turing instability of the stationary state (U_+, V_+) (which takes place if $c = 0$) or Turing–Hopf instability ($c \neq 0$), the homogeneous equilibrium becomes unstable with respect to periodic perturbations for $a < a_*$. If the instability is supercritical, one

expects a small band of stable patterns, the so-called Eckhaus-band for $|a - a_*| = \mathcal{O}(\varepsilon^2)$ and $0 < \varepsilon \ll 1$.

In this section we will derive and analyze the associated Ginzburg–Landau equations for the GKGS-model in each of the four classes of Fig. 1 and for the special cases of Proposition 2. The Ginzburg–Landau equation (GLE) governs the behavior of the amplitude of the pattern near criticality. Solutions to this equation are slow modulations of the amplitude of the underlying 'most unstable' Fourier mode $\sim e^{i(k_* x + \omega_* t)}$ (see Aranson and Kramer 2002; Mielke 2002 and the references therein).

In the case of the Gray–Scott system it is shown in Morgan et al. (2000) that the Turing instability is supercritical, meaning that stable small amplitude periodic solutions exist in the region where the underlying homogeneous pattern is unstable. In Sect. 2.5 we derive that for $\gamma > \gamma_* \approx 13$ and $c = 0$, the Turing instability of the stationary state (U_+, V_+) of the GKGS-model becomes subcritical (however, we cannot think of a relevant ecological interpretation of these values for γ). We also find that the Turing–Hopf instability that occurs for $c \neq 0$ is supercritical for all values of c and either $\gamma = 1$ or $\gamma = 2$.

In Sect. 2.6 it is shown that, near criticality, the Klausmeier system can be derived as a limit case of the GKGS-system for $c \to \infty$ (in particular, $0 < 1/\sqrt{c} \ll \varepsilon^2 \ll 1$). It is explained that the GLE for the Klausmeier model is the same as the limiting GLE for the GKGS-system for large c and asymptotically small $|\varepsilon| \ll 1$ (that is, we assume $0 < \varepsilon^2 \ll 1/\sqrt{c} \ll 1$). This is surprising: a priori, it is not at all clear that it is possible to interchange the limits $\varepsilon \to \infty$ and $c \to \infty$. In particular, the Turing–Hopf instability of the background state (U_+, V_+) of the Klausmeier system inherits the supercriticality from the Turing–Hopf instability of the background state of the GKGS-model.

Let $0 < \varepsilon \ll 1$ and assume that the stationary state (U_+, V_+) is almost marginally unstable ($a = a_* - r\varepsilon^2$, $r > 0$). Patterns close to the stationary state (U_+, V_+) can be described by

$$\begin{aligned} U &= \delta^{2\beta-\alpha}\big(\hat{U}_+ + \varepsilon \hat{U}(x,t)\big), \\ V &= \delta^{\alpha-\beta}\big(\hat{V}_+ + \varepsilon \hat{V}(x,t)\big). \end{aligned} \tag{2.36}$$

By substitution of these expressions in (1.5) and recalling the previous scaling for ν in (2.18) and the previous scalings for $\tilde{k}$ and $\tilde{\lambda}$ that induce the spatial and temporal scalings

$$\tilde{x} = x\delta^{\frac{1}{2}\alpha - \frac{1}{2}(2\beta-\alpha)\gamma} \quad \text{and} \quad \tilde{t} = t\delta^{\beta}, \tag{2.37}$$

we deduce the following leading order system for the GKGS-system:

$$
\begin{aligned}
\delta^{3\beta-2\alpha}U_t &= \gamma\left(\frac{b^2}{a_*}\right)^{\gamma-1}U_{xx} + cU_x - \left[\frac{a_*^2}{b^2}U + 2bV\right] \\
&\quad + \varepsilon\left[\gamma(\gamma-1)\left(\frac{b^2}{a_*}\right)^{\gamma-2}\left[U_{xx}U + (U_x)^2\right] - \frac{b^2}{a_*}V^2 - 2\frac{a_*}{b}UV\right] \\
&\quad + \varepsilon^2\left[\gamma(\gamma-1)(\gamma-2)\left(\frac{b^2}{a_*}\right)^{\gamma-3}\left[U(U_x)^2 + \frac{1}{2}U^2U_{xx}\right]\right. \\
&\quad \left. + \gamma(\gamma-1)\frac{1}{a_*}\left(\frac{b^2}{a_*}\right)^{\gamma-1}U_{xx} + 2r\frac{a_*}{b^2}U - UV^2\right], \\
V_t &= V_{xx} + \left[\frac{a_*^2}{b^2}U + bV\right] + \varepsilon\left[\frac{b^2}{a_*}V^2 + 2\frac{a_*}{b}UV\right] - \varepsilon^2\left[2r\frac{a_*}{b^2}U - UV^2\right],
\end{aligned}
\tag{2.38}
$$

where we have dropped all hats and tildes and have implicitly assumed $\delta \ll \varepsilon$. Remark that after application to the linearly 'most unstable' Fourier mode $\sim e^{i(k_*x+\omega_* t)}$, the leading order part of (2.38) indeed corresponds to $\mathcal{M}_{i\omega_*}(a_*, c, ik_*)$ (see (2.21)). The kernel of $\mathcal{M}_{i\omega_*}(a_*, c, ik_*)$ is given by

$$
\ker \mathcal{M}_{i\omega_*}(a_*, c, ik_*) = \begin{pmatrix} 2b \\ \eta_{\gamma,c} \end{pmatrix}, \tag{2.39}
$$

with

$$
\eta_{\gamma,c} := -\Gamma k_*^2 - \left(\frac{a_*}{b}\right)^2 + ik_*c, \tag{2.40}
$$

and the range of $\mathcal{M}_{i\omega_*}(a_*, c, ik_*)$ is given by

$$
\operatorname{Rg} \mathcal{M}_{i\omega_*}(a_*, c, ik_*) = \begin{pmatrix} -2b \\ -k_*^2 + b - i\omega_* \end{pmatrix}. \tag{2.41}
$$

Thus, $\mathcal{M}_{i\omega_*}(a_*, c, ik_*)\mathbf{x} = \mathbf{y}$ has a solution if and only if $\mathbf{y} \in \operatorname{Rg} \mathcal{M}_{i\omega_*}(a_*, c, ik_*)$, that is, if and only if

$$
2by_2 - \left(k_*^2 + i\omega_* - b\right)y_1 = 0, \tag{2.42}
$$

where $\mathbf{y} = (y_1, y_2)^{\mathrm{T}}$. We will need this in our derivation of the GLE and refer to it as the *solvability condition*.

The modulation Ansatz for the derivation of the Ginzburg–Landau equation is that solutions of the system behave as slow spatio-temporal modulations of the solution for the linear first order problem, i.e., they are of the form:

$$
\begin{pmatrix} U \\ V \end{pmatrix} = \mathcal{A}(\xi, \tau)\begin{pmatrix} 2b \\ \eta_{\gamma,c} \end{pmatrix} e^{i(k_*x+\omega_* t)} + \text{c.c.} + \text{h.o.t.}, \tag{2.43}
$$

with $\xi = \varepsilon x$ and $\tau = \varepsilon^2(x - c_g t)$ and c_g the group velocity defined by (2.26) (Aranson and Kramer 2002; Mielke 2002).

In Morgan et al. (2000) the GLE for periodic patterns near the Turing instability of the background state (U_+, V_+) for the Gray–Scott system was computed. Using

a result of Schneider (1998), the diffusive stability of the Turing patterns described by the Gray–Scott system could be derived from the spectral stability of periodic solutions of this GLE. However, to our knowledge there does not exist a similar result in the literature that can be applied to the present system, i.e., a quasilinear reaction–diffusion system with nonlinear diffusion. In fact, we are not aware of any (even formal) GLE analysis in a system with nonlinear diffusion. Still, we expect that a result similar to that of Schneider (1998) must hold—although a proof is beyond the scope of this paper. The reason for this is that the nonlinear diffusion term in (1.5) can be controlled if U remains bounded away from 0, i.e., if $U(x,t) \geq d_0 > 0$ uniformly in x and t. By the nature of the method, the GLE analysis is applied to solutions $(U(x,t), V(x,t))$ of (1.5) that are asymptotically close to the background state (U_+, V_+) of (1.5), as is made explicit by 'Ansatz' (2.36). Since clearly $U_+ > 0$ (see also (2.2)), the GLE approach indeed only considers patterns in (1.5) for which $U(x,t) \geq d_0 > 0$ uniformly in x and t on the time scales associated to this approach. In this region the equation is still parabolic and existence theory is essentially similar to the semilinear case—see Remark 2.

In Sect. 2.5 we derive a Ginzburg–Landau equation for the slowly varying amplitude $\mathcal{A}(\xi,\tau)$. The Ginzburg–Landau equation is first derived without inserting explicit values of a_* and k_*. The coefficients of the GLE are functions of b, c, and γ, as it is proven in Proposition 2 that the critical values of a_* and k_* depend on b, c, and γ. In Proposition 2 however, we also deduced explicit values for a_* and k_* for a number of special parameter values for b, c, and γ. In each of these cases, we will present an explicit GLE.

2.5 Ginzburg–Landau Equation for the GKGS-Model

Proposition 3 *Assume $|a - a^*| = r\varepsilon^2$ and $\varepsilon > 0$ small enough. Then, the Ginzburg–Landau equation associated to (1.5) for solutions of the form (2.43) near the Turing–Hopf instabilities of Proposition 2 has the form*

$$\mathcal{A}_\tau = (a_1 + \mathrm{i}a_2)\mathcal{A}_{\xi\xi} + (b_1 + \mathrm{i}b_2)\mathcal{A} + (L_1 + \mathrm{i}L_2)|\mathcal{A}|^2\mathcal{A} \tag{2.44}$$

with coefficients given by

$$\begin{aligned}
a_1 + \mathrm{i}a_2 &= \frac{1}{2b\eta_{\gamma,c}}\big[2b(\mathrm{c_g}y_{12} + \eta_{\gamma,c} + 2\mathrm{i}k_* y_{12}) \\
&\quad - \big(k_*^2 + \mathrm{i}\omega_* - b\big)(cx_{12} + 2b\Gamma + 2\mathrm{i}k_*\Gamma x_{12})\big], \\
b_1 + \mathrm{i}b_2 &= \frac{-1}{2b\eta_{\gamma,c}}\left[4\frac{a_c}{b}\big(k_*^2 + \mathrm{i}\omega_* + b\big) + L_{\mathcal{A},\mathrm{NLD}}\big(k_*^2 + \mathrm{i}\omega_* - b\big)\right], \\
L_1 + \mathrm{i}L_2 &= \frac{1}{2b\eta_{\gamma,c}}\big[\big(k_*^2 + \mathrm{i}\omega_* + b\big)L_{\mathrm{tot}} - \big(k_*^2 + \mathrm{i}\omega_* - b\big)L_{\mathrm{NLD}}\big].
\end{aligned} \tag{2.45}$$

We refer to the Appendix for the detailed derivation of the GLE as well as the full expressions for L_{tot}, L_{NLD} and $L_{\mathcal{A},\mathrm{NLD}}$, and x_{ij}, y_{ij}, $ij = 02, 12, 13$. Here we remark that if $c = 0$, then $\omega_* = 0$ and $c_\mathrm{g} = 0$ by (2.26) and $L_{\mathrm{NLD}} = 0$ and $L_{\mathcal{A},\mathrm{NLD}} = 0$ if $\gamma = 0$, i.e., these coefficients originate from the nonlinear diffusion.

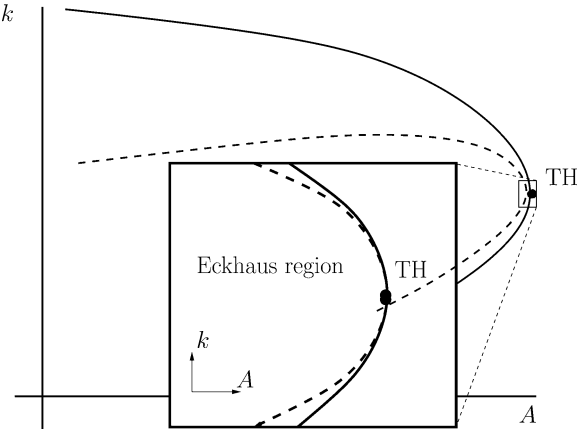

Fig. 4 An impression of the stable Eckhaus region as part of a Busse balloon. Compare Fig. 2. *Inset*: the Eckhaus region of stable patterns (boundary depicted by a *dashed line*) lies within the larger locally parabolic region of (not necessarily stable) patterns

In the GLE (2.44), the coefficient $L_1 + \mathrm{i}L_2$ is called the Landau-coefficient. The Turing–Hopf instability of the stationary state (U_+, V_+) is supercritical if and only if its real part satisfies $L_1 < 0$. It is subcritical if $L_1 > 0$.

If the Turing–Hopf bifurcation is supercritical, it is straightforward to show (Matkowsky and Volpert 1993) that there exists a band of stable spatially periodic patterns if and only if

$$1 + \frac{a_2 L_2}{a_1 L_1} > 0. \tag{2.46}$$

This inequality is usually called the *Benjamin–Feir–Newell criterion* (Aranson and Kramer 2002). The patterns that satisfy condition (2.46) form a parabolically shaped region of stable periodic patterns near the Turing(–Hopf) instability at $a = a_*$ that lies within a larger parabolically shaped region of periodic patterns (Matkowsky and Volpert 1993; Mielke 2002). See Fig. 4 for a schematic picture. For $a \approx a_* - r\varepsilon^2$, the region of stable patterns is called the *Eckhaus region*, after its boundary which is called the Eckhaus instability (Mielke 2002). In Fig. 4 the Eckhaus region is depicted as a part of the larger Busse balloon (the concept of the Busse balloon will be discussed in depth in Sect. 3).

As explained in the introduction, the ecologically relevant parameter values for γ are $\gamma = 1$ or $\gamma = 2$. With the help of MATHEMATICA we evaluated the Landau coefficient of the GLE for the GKGS-model with $\gamma = 1$ and $\gamma = 2$. This way, we have obtained sufficient evidence to claim:

Claim 1 *For the GKGS-model (1.5) with $\gamma \in \{1, 2\}$, the real part of the Landau coefficient L_1 of (2.44) is negative for all values of b and c up to $c \sim 10^6$ and $b \sim 10^2$. Therefore we claim that the Turing–Hopf bifurcation at $a = a_*$ of the stationary state (U_+, V_+) of the GKGS-model with $c > 0$ and $\gamma = 1, 2$ is supercritical.*

As an illustration, we have depicted in Fig. 5 a set of contourlines of the real part of the Landau-coefficient L_1 for $\gamma = 1$ and $\gamma = 2$ and values of (b, c) on a grid spanned by $(b, c) = (0.1, 0.0) + 0.1(k, l)$, $k, l = 0, \ldots, 40$.

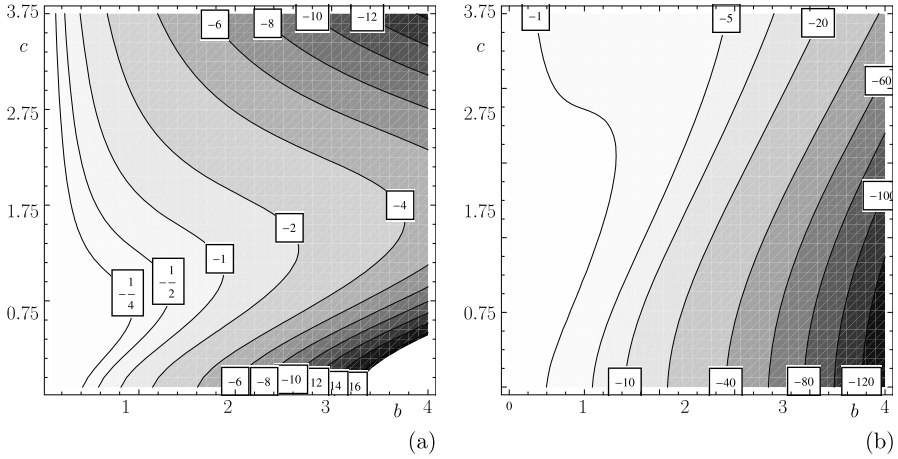

Fig. 5 Contourplots of the real part of the Landau-coefficient for (**a**) the GKGS-model with linear diffusion ($\gamma = 1$) and for (**b**) the GKGS-model with nonlinear diffusion ($\gamma = 2$), drawn on a grid of points at $(b, c) = (0.1, 0.0) + 0.1(k, l)$, $k, l = 0, \ldots, 40$. In both pictures, the non-advection case ($c = 0$) is depicted by the horizontal axis. Notice that the origin in the pictures is at $(b, c) = (0.1, 0.0)$, since the case $b = 0$ has no ecological meaning

By computing the Benjamin–Feir–Newell criterion (2.46), we checked that this inequality holds for the Ginzburg–Landau equation for the GKGS-model for all b and c up to $c \sim 10^6$ and $b \sim 10^2$ and $\gamma \in \{1, 2\}$. Hence we claim the following.

Claim 2 *For* (1.5) *with* $c > 0$ *and* $\gamma = 1, 2$, *there exists a stable band of periodic patterns that appears at the Turing–Hopf instability.*

Next, we present four explicit Ginzburg–Landau equations for which we have explicit values for the critical parameter value a_* and wavenumber k_* at hand. The parameter choices for the three Ginzburg–Landau equations are drawn from three different cases of the GKGS-model as depicted in Fig. 1. Of course, the sign of the real part of the Landau coefficient confirms the evaluations presented in Fig. 5 in all three cases.

2.5.1 The GKGS-Model with $c = 0$ and $\gamma = 1$

Clearly, the GKGS-model with $\gamma = 1$ and $c = 0$ reduces to the Gray–Scott system. By recalling from Proposition 1 (or from Morgan et al. 2000), $a_*^2 = (3 - 2\sqrt{2})b^3$ and $k_*^2 = (\sqrt{2} - 1)b^3$, the above equation simplifies to

$$\mathcal{A}_\tau = 2\sqrt{2}\mathcal{A}_{\xi\xi} + \frac{2}{\sqrt{b}}\mathcal{A} - \frac{2}{9}(10\sqrt{2} - 7)b^2|\mathcal{A}|^2\mathcal{A}. \tag{2.47}$$

Since the real part of the Landau coefficient is negative, the Turing-bifurcation is supercritical. Note that this equation corresponds to (3.27) derived in Morgan et al. (2000).[1]

2.5.2 *The GKGS-Model with $c = 0$*

In the case of $c = 0$ and $\gamma \geq 1$, we have derived explicit expressions for the critical parameter a_* and wavenumber k_* in Proposition 1, namely

$$a_*^{\gamma+1} = g\gamma b^{2\gamma+1} \quad \text{and} \quad k_*^2 = \frac{1}{2}(1-g)b, \tag{2.48}$$

with $g = 3 - 2\sqrt{2}$ (notice we rescaled k_* in Sect. 2.3). Due to the reflection symmetry of the GKGS-system at $c = 0$, all coefficients of the GLE are real. In this case, the GLE (2.44) has the form

$$\mathcal{A}_\tau = 2\sqrt{2}\,\mathcal{A}_{\xi\xi} + b_1(\gamma)\mathcal{A} + L_1(\gamma)|\mathcal{A}|^2\mathcal{A} \tag{2.49}$$

with

$$b_1(\gamma) = \left[39 - 27\sqrt{2} - (41 - 29\sqrt{2})\gamma\right]\left(\frac{g\gamma}{b}\right)^{-1/(1+\gamma)}\frac{1}{b},$$

$$L_1(\gamma) = -\frac{1}{9}(2-\sqrt{2})\left[18(3+2\sqrt{2}) + 12(2+\sqrt{2})\gamma + (-8+3\sqrt{2})\gamma^2\right] \times \left(\frac{g\gamma}{b}\right)^{\frac{2}{\gamma+1}} b^3.$$

One can check that $b_1(\gamma) > 0$ for $\gamma > 0$ as it—of course—should. Moreover, the Ginzburg–Landau equation for the GKGS-system for general γ (2.49) reduces to the Ginzburg–Landau equation for the Gray–Scott system (2.47) if $\gamma = 1$.

However, we notice that the (real) Landau coefficient $L_1(\gamma)$ becomes positive for large γ and equals zero for

$$\gamma_{ss} \approx 13.0446. \tag{2.50}$$

Therefore we have the following result.

Proposition 4 *The Turing bifurcation for the GKGS-model* (1.2) *with $c = 0$ is supercritical for $\gamma < \gamma_{ss}$ and subcritical for $\gamma > \gamma_{ss}$.*

[1] Notice however the extra b^2 in the coefficient in front of the nonlinear term. In Morgan et al. (2000), b is scaled out of the matrix $\mathcal{M}_c$ in formula (3.24). That is, the matrix $b\mathcal{M}_c$ in Morgan et al. (2000) plays the role of our matrix $\mathcal{M}_{i\omega_c}(a_c, 0, ik_c)$. This is equivalent to scaling $\mathcal{A} \to b\mathcal{A}$ in (2.47).

2.5.3 *The Ginzburg–Landau Equation for the GKGS-Model with $\gamma = 1$ and $c = \sqrt{\frac{2}{3}b}$*

In this case, the critical parameters for the Turing–Hopf instability can be drawn from the 'special case' in Proposition 2:

$$k_*^2 = \frac{1}{3}b, \quad a_*^2 = \frac{1}{3}b^3, \quad \omega_* = \frac{1}{3}b\sqrt{2}, \quad \text{and} \quad c_g = \sqrt{\frac{2}{3}b}.$$

The GKGS-model for $\gamma = 1$ is not reflection symmetric. Therefore, traveling spatially periodic patterns appear in a Turing–Hopf bifurcation. The associated GLE is a complex GLE (cGLE),

$$\mathcal{A}_\tau = \frac{1}{3}(8 + \mathrm{i}\sqrt{2})\mathcal{A}_{\xi\xi} + \frac{2}{9}\sqrt{\frac{3}{b}}(5 + \mathrm{i}\sqrt{2})\mathcal{A} - \frac{2}{33}(5 - 2\mathrm{i}\sqrt{2})b^2|\mathcal{A}|^2\mathcal{A}. \tag{2.51}$$

Since $\mathrm{Re}(-\frac{2}{33}(5 - 2\mathrm{i}\sqrt{2})b^2) < 0$, the bifurcation is supercritical. We refer to Appendix A.1 for a complete derivation. We remark that it is possible to derive a special case GLE for general γ (see Proposition 2). However, this gives no additional insight.

2.6 Ginzburg–Landau Equation for the Case $c \gg 1$: The Klausmeier Model and the GKGS Model for $c \gg 1$

In the Gray–Scott scaling introduced in (1.5), the original Klausmeier system reads[2]

$$\begin{cases} U_t = U_x + A(1 - U) - UV^2, \\ V_t = \delta^{2\sigma} V_{xx} - BV + UV^2. \end{cases} \tag{2.53}$$

Of course, the stationary states for the Klausmeier system are the same as the stationary states for the GKGS-model: we have the 'desert' state (U_0, V_0) and the stationary states $(U_\pm, V_\pm)$ given in (1.6).

A priori, (2.53) cannot be considered as a natural limit of the GKGS-system (1.5) since the diffusion coefficient d_u in front of U has been scaled to $d_u = 1$ in (1.5) (so d_u cannot be set to 0). In fact, from the point of view of mathematical modeling the original Klausmeier system is somewhat inconsistent: the (linear or nonlinear) diffusion of water U is neglected since it is dominated by the advection term, while the diffusion of vegetation V, which is in fact much smaller than that of U, is retained in (2.53).

[2] Notice that this rescaling of the Klausmeier system can be acquired from Klausmeier's original nondimensional system (see Klausmeier 1999),

$$\begin{cases} u_T = \nu u_X + a - u - uv^2; \\ v_T = \delta^{2\sigma} v_{XX} - mv + uv^2, \end{cases} \tag{2.52}$$

by rescaling with $x = \frac{a^2}{\nu}X$, $t = a^2 T$, $v = aV$, $u = aU$, $A = \frac{1}{a^2}$, $B = \frac{m}{a^2}$ and by further introducing $0 < \delta^\sigma := \frac{a}{\nu} \ll 1$. (From the estimates for a and ν in Klausmeier (1999), it can be deduced that indeed $0 < \frac{a}{\nu} \ll 1$.)

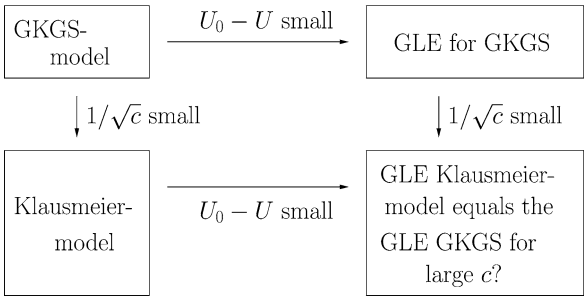

Fig. 6 Diagram for the GLE for the GKGS for large c and the GLE for the Klausmeier-model. A priori, it is unclear whether this diagram commutes

In this subsection we justify this for $C \gg 1$ in (1.5) or $c \gg 1$ in (2.38) and discuss the relation between the GKGS model with $c \gg 1$, i.e., the case in which advection dominates diffusion in the U-equation, with the original Klausmeier model. We will do so in the context of the 'rise of patterns' and handle the problem in terms of the GLE associated to the Turing–Hopf bifurcations. As shown in the diagram of Fig. 6, there are two paths to obtain a GLE for the case $c \gg 1$. Based on the previous sections, the most direct way is to consider the case $c \gg 1$ in the general GLE with coefficients given by (2.45) by introducing a new small parameter $1/\sqrt{c}$. This choice implies that it is implicitly assumed that $0 < \varepsilon \ll 1/\sqrt{c} \ll 1$ (recall that ε is the distance from criticality introduced in Sect. 2.3).

However, we will first start out with a path that is closer to the original motivation behind the Klausmeier model: before we embark upon the weakly nonlinear GLE analysis, we first consider the limit $c \gg 1$ in (1.5). In other words, we take the other path in Fig. 6 and assume that $0 < 1/\sqrt{c} \ll \varepsilon \ll 1$. We show that under this assumption the GKGS equation indeed agrees exactly with the Klausmeier model (at leading order). Nevertheless, this limit is significantly different from the limit associated to the other path in the diagram of Fig. 6 and there is a priori no reason for the diagram in Fig. 6 to commute. The somewhat surprising outcome to our analysis is that the two resulting GLEs are identical. Before we consider asymptotically large $c \gg 1$, we introduce the scalings

$$\begin{aligned} &U = \frac{\tilde{U} b^{3/4}}{\sqrt{c}}; \qquad V = b^{1/4}\sqrt{c}\tilde{V}; \qquad a_* = \tilde{a}_* b^{5/4}\sqrt{c}; \\ &x = b^{-1/2}\tilde{x}; \qquad t = b^{-1/4}\tilde{t}; \qquad r = \tilde{r} b^{5/4}\sqrt{c}. \end{aligned} \tag{2.54}$$

These rescalings here appear a little abruptly. We remark, however, that it follows from Proposition 2 that a_* grows with $\sqrt{c}$ as $c \gg 1$ and that the rescalings in terms of c are 'balanced' such that the terms resulting from the nonlinear diffusion in the U-component of the GKGS-system for $\gamma \geq 1$ are of higher order in $1/\sqrt{c}$ and such that all other terms are of the same, lowest order. The rescalings with b are balanced such that all terms in the GKGS-model that are of lowest order in $1/\sqrt{c}$ are also of the same order in b. We refer to Appendix A.3 for a more elaborate account on the derivation of these rescalings.

Now, starting from the GKGS model we employ the following scalings. As before, we rescale $\tilde{x}$ and $\tilde{t}$ in the GKGS-model (1.5) as given by (2.37). In Sect. 2.4, we have

seen that patterns close to the stationary state given by (2.36) are described by the leading order form (2.38) with respect to ε. We adopt the rescalings as given in (2.54) and obtain, by disregarding all terms that are of higher order in $1/\sqrt{c}$,

$$\begin{aligned} 0 &= \tilde{U}_{\tilde{x}} - \left[\tilde{a}_*^2\tilde{U} + 2\tilde{V}\right] - \varepsilon\left[\frac{1}{\tilde{a}_*}\tilde{V}^2 + 2\tilde{a}_*\tilde{U}\tilde{V}\right] + \varepsilon^2\left[2\tilde{r}\tilde{a}_*\tilde{U} - \tilde{U}\tilde{V}^2\right], \\ \tilde{V}_{\tilde{t}} &= \tilde{V}_{\tilde{x}\tilde{x}} + \left[\tilde{a}_*^2\tilde{U} + \tilde{V}\right] + \varepsilon\left[\frac{1}{\tilde{a}_*}\tilde{V}^2 + 2\tilde{a}_*\tilde{U}\tilde{V}\right] - \varepsilon^2\left[2\tilde{r}\tilde{a}_*\tilde{U} - \tilde{U}\tilde{V}^2\right]. \end{aligned} \tag{2.55}$$

Note that the leading order formulation of the GKGS-system for large c presented in (2.55) does not include any terms that result from the nonlinear diffusion in the U-component. In ecological terms this confirms the (natural) observation that the character of the diffusion is irrelevant in a strongly sloped—and thus advection dominated—setting.

It is easy to verify that the leading order system (2.55) is identical to the one that could be derived from the Klausmeier system (2.52), had we adopted the rescalings given in (2.54) with $c = 1$ (as is the case in (2.53)). Thus, the system (2.55) also describes the dynamics of the Klausmeier system near the Turing–Hopf instability of (U_+, V_+). Therefore, we indeed have deduced that the Klausmeier model coincides with the GKGS model (at leading order) if we assume that $0 < 1/\sqrt{c} \ll \varepsilon \ll 1$.

Now we turn to the GLE analysis. In Appendix A.3, it is shown that the associated GLE is given by

$$\begin{aligned} \mathcal{A}_\tau = {} & \frac{1}{41}\left[(66 - 56\sqrt{2}) - \mathrm{i}(63 - 23\sqrt{2})\sqrt{\sqrt{2} - 1}\right]\mathcal{A}_{\xi\xi} \\ & + \tilde{r}\left[4\sqrt{\sqrt{2} - 1} + \mathrm{i}(4 - 2\sqrt{2})\right]\mathcal{A} \\ & + \frac{4}{69}\left[-807 + 534\sqrt{2} + \mathrm{i}(418 - 286\sqrt{2})\sqrt{\sqrt{2} - 1}\right]|\mathcal{A}|^2\mathcal{A}. \end{aligned} \tag{2.56}$$

Numerically, the Landau-coefficient in front of the $|\mathcal{A}|^2\mathcal{A}$-term is given by

$$L_{|\mathcal{A}|^2\mathcal{A}} \approx -1.50174 + 0.252493\,\mathrm{i}.$$

We see that the real part of the Landau-coefficient is negative. This once more confirms that the Turing–Hopf bifurcation of the equilibrium (U_+, V_+) in the Klausmeier model is supercritical. We note that this establishes the supercriticality of the Turing–Hopf instability of the background state (U_+, V_+) that was suggested in Sherratt and Lord (2007).

Next, we consider the alternative path in the diagram given in Fig. 6 and assume $0 < \varepsilon \ll 1$. In order to obtain an end result that can be compared to the other path, we

scale (2.38) with (2.54) for $c \neq 0$ (i.e., not necessarily $c \gg 1$) and obtain

$$\begin{aligned}
&\delta^{3\beta-2\alpha} b^{\frac{1}{2}} c^{-\frac{1}{2}} \tilde{U}_{\tilde{t}} \\
&\quad = \gamma \tilde{a}_*^{1-\gamma} b^{\frac{3}{4}\gamma-\frac{1}{4}} c^{-\frac{1}{2}\gamma} \tilde{U}_{\tilde{x}\tilde{x}} + c^{\frac{1}{2}} \tilde{U}_{\tilde{x}} - c^{\frac{1}{2}} \big[a_*^2 \tilde{U} + 2\tilde{V}\big] \\
&\qquad + \varepsilon \Bigg[\gamma(\gamma-1) \tilde{a}_*^{2-\gamma} b^{\frac{3}{4}\gamma-\frac{1}{4}} c^{-\frac{1}{2}\gamma} \big[\tilde{U}_{\tilde{x}\tilde{x}} U + (\tilde{U}_{\tilde{x}})^2\big] - c^{\frac{1}{2}} \Big[\frac{1}{\tilde{a}_*} V^2 + 2\tilde{a}_* \tilde{U} \tilde{V} \Big] \Bigg] \\
&\qquad + \varepsilon^2 \Bigg[\gamma(\gamma-1)(\gamma-2) \tilde{a}_*^{3-\gamma} b^{\frac{3}{4}\gamma-\frac{1}{4}} c^{-\frac{1}{2}\gamma} \Big[\tilde{U} (\tilde{U}_{\tilde{x}})^2 + \frac{1}{2} \tilde{U}^2 \tilde{U}_{\tilde{x}\tilde{x}} \Big] \\
&\qquad + \gamma(\gamma-1) \tilde{a}_*^{-\gamma} b^{\frac{3}{4}\gamma-\frac{3}{2}} c^{-\frac{1}{2}\gamma-\frac{1}{2}} \tilde{U}_{\tilde{x}\tilde{x}} + 2r\tilde{a}_* c^{\frac{1}{2}} \tilde{U} - c^{\frac{1}{2}} \tilde{U} \tilde{V}^2 \Bigg]; \\
&\tilde{V}_{\tilde{t}} = \tilde{V}_{\tilde{x}\tilde{x}} + \big[\tilde{a}_*^2 \tilde{U} + \tilde{V}\big] + \varepsilon \Big[\frac{1}{a_*} \tilde{V}^2 + 2a_* \tilde{U} \tilde{V} \Big] - \varepsilon^2 \big[2r\tilde{a}_* \tilde{U} - \tilde{U} \tilde{V}^2\big].
\end{aligned} \tag{2.57}$$

In Appendix A.3 we derive that for asymptotically large c, the GLE for this system equals the GLE for the Klausmeier system (2.56). Therefore, patterns near the Turing–Hopf point of the GKGS-system for large c are, to first order, described by the Klausmeier system. Ecologically, one may put this by saying that ecosystems for which the slope along which the water flows downhill has a relatively steep gradient, are, to first order, described by the Klausmeier model.

3 Busse Balloons for the Generalized Klausmeier–Gray–Scott Model

The Ginzburg–Landau analysis of the last section is weakly nonlinear in the sense that it is valid only given the necessary assumption that the parameter a is close to its critical value a_* at which the Turing(–Hopf) bifurcation takes place, that is, $|a - a_*| = \mathcal{O}(\varepsilon^2)$ for a small parameter $0 < \varepsilon \ll 1$. Naturally, we are interested in the existence of stable patterns if a is not asymptotically close to a_*. In this section, by using novel techniques implemented in the continuation software package AUTO (Doedel 2007), we will present a complete picture of all the instabilities that spatially periodic patterns can undergo for different values of a and fixed values for b, c, and γ. This complete picture will be called the Busse balloon, after the physicist F. Busse who introduced the concept in Busse (1978). Later, mostly partial presentations of Busse balloons for reaction–diffusion systems had been presented, see Chossat and Iooss (1994), Eckhaus and Iooss (1989), Morgan et al. (2000) and the references therein. To our knowledge, the first complete Busse balloon has been described in Doelman et al. (2012). In this section, we will give a description of a series of Busse balloons for the GKGS-model. See also Fig. 4, in which we have depicted the Eckhaus region as part of the larger Busse balloon.

To be more precise, let us consider the GKGS-system (1.5) for some fixed B, C, and γ and let, as before, κ be the nonlinear wavenumber.[3] A *Busse balloon* for the

[3]Note that we silently switched back to the original parameters A, B, and C in (1.5). We will comment on the relation between A, B, and C on the one hand and a, b, and c on the other hand in Sect. 3.2.

GKGS-system (1.5) for B, C, and γ is a (not necessarily connected) set $\mathcal{B}$ in (A,κ)-space with the following property: a point (A,κ) lies in $\mathcal{B}$ if Eq. (1.5) with parameter A allow for at least one stable periodic solution (U_p, V_p) with wavenumber κ. Periodic patterns on the boundary of a Busse balloon ∂B are marginally stable.

The Busse balloon is part of the larger realm of existing (i.e., not necessarily stable) patterns. Let us give a proper definition for the convenience of terminology. The *existence region* or *existence balloon* is a (not necessarily connected) set $\mathcal{E}$ in (A,κ)-space with the following property: a point (A,κ) lies in $\mathcal{E}$ if Eq. (1.5) with parameter A allow for at least one periodic solution (U_p, V_p) with wavenumber κ. Typically, this means that the set has nonempty interior (Rademacher and Scheel 2007).

In this section, we present a series of Busse balloons for a number of choices for the values of B, C, and γ (we will explain our choices for the values of these parameters later). First, we briefly present some facts from the stability theory of wave trains. Then, we consider the instabilities that will appear in the construction of the Busse balloons in the next section. Thirdly, we explain the numerical continuation method.

Stability of Wave Trains The GKGS-system (1.5) can be recast in a moving frame of reference, with respect to the variables $(\xi,t)=(x-st,t)$ (and with a slight abuse of notation),

$$\begin{cases} U_t = \left(U^\gamma\right)_{\xi\xi} + (s+C)U_\xi + A(1-U) - UV^2, \\ V_t = DV_{\xi\xi} + sU_\xi - BV + UV^2. \end{cases} \tag{3.1}$$

The basic advantage here is that generic wave trains $u_{\mathrm{per}}(\xi)=(U_{\mathrm{per}}(\xi), V_{\mathrm{per}}(\xi))$ with $\xi=\kappa x+\Omega t$ and $u_{\mathrm{per}}(\xi)=u_{\mathrm{per}}(\xi+2\pi)$ then become stationary L-periodic solutions for $s=\Omega/\kappa$ (and with $L=2\pi/\kappa$),

$$\begin{cases} 0 = \left(U_{\mathrm{per}}^\gamma\right)_{\xi\xi} + (s+C)U_{\mathrm{per},\xi} + A(1-U_{\mathrm{per}}) - U_{\mathrm{per}}V_{\mathrm{per}}^2, \\ 0 = DV_{\mathrm{per},\xi\xi} + sU_{\mathrm{per},\xi} - BV_{\mathrm{per}} + U_{\mathrm{per}}V_{\mathrm{per}}^2. \end{cases} \tag{3.2}$$

To establish spectral stability, we linearize (3.1) about $u_{\mathrm{per}}=(U_{\mathrm{per}}, V_{\mathrm{per}})$ by perturbing the wave train with $u(\xi)\mathrm{e}^{\lambda t}$. We obtain the linear problem (write $u=(U,V)$),

$$\begin{cases} \lambda U = \gamma U_{\mathrm{per}}^{\gamma-1}U_{\xi\xi} + D_1U_\xi - D_2U - 2U_{\mathrm{per}}V_{\mathrm{per}}V, \\ \lambda V = DV_{\xi\xi} + sV_\xi + V_{\mathrm{per}}^2U - (B-2U_{\mathrm{per}}V_{\mathrm{per}})V, \end{cases} \tag{3.3}$$

with $D_1 = D_1[U_{\mathrm{per}},\gamma,s,C] := \gamma(\gamma-1)U_{\mathrm{per}}U_{\mathrm{per},\xi\xi}^{\gamma-2} + \gamma(\gamma-1)(\gamma-2)U_{\mathrm{per}}^2U_{\mathrm{per},\xi\xi}^{\gamma-3} + s + C$ and $D_2 = D_2[U_{\mathrm{per}},U_{\mathrm{per}},\gamma,A,] := 2\gamma(\gamma-1)U_{\mathrm{per}}U_{\mathrm{per},\xi\xi}^{\gamma-2} + A + V_{\mathrm{per}}^2$. Written as a first-order ODE, (3.3) defines a four-component system

$$\phi_\xi = \mathcal{A}_\lambda\left(u_{\mathrm{per}}(\xi)\right)\phi \tag{3.4}$$

with

$$\mathcal{A}_\lambda\big(u_{\mathrm{per}}(\xi)\big) = \begin{pmatrix} 0 & 1 & 0 & 0 \\ \frac{\lambda+D_2}{\gamma U_{\mathrm{per}}^{\gamma-1}} & -\frac{D_1}{\gamma U_{\mathrm{per}}^{\gamma-1}} & \frac{2U_{\mathrm{per}}V_{\mathrm{per}}}{\gamma U_{\mathrm{per}}^{\gamma-1}} & 0 \\ 0 & 0 & 0 & 1 \\ -\frac{V_{\mathrm{per}}^2}{D} & 0 & \frac{\lambda+B-2U_{\mathrm{per}}V_{\mathrm{per}}}{D} & -\frac{s}{D} \end{pmatrix}. \tag{3.5}$$

The matrix $\mathcal{A}_\lambda(u_{\mathrm{per}}(\xi))$ is L-periodic. Hence, by Floquet theory, there exists an L-periodic matrix $\mathcal{B}_\lambda(\xi)$ and a constant matrix $\mathcal{R}_\lambda$ such that the fundamental solution to the above first-order system is given by

$$\Phi_\lambda(\xi) = \mathcal{B}_\lambda(\xi)\mathrm{e}^{\mathcal{R}_\lambda \xi}.$$

Since we only allow for bounded perturbations, it follows that the Floquet exponents ν of Φ_λ are purely imaginary, $\nu = \mathrm{i}k$. That is, the dispersion relation

$$d(\lambda, \mathrm{i}k) := \det\big(\Phi_\lambda(L) - \mathrm{e}^{\mathrm{i}kL} I\big) = 0 \quad \text{for some } k \tag{3.6}$$

holds. This is equivalent to the boundary value problem (see Rademacher et al. 2007)

$$\begin{aligned} \lambda u &= \mathcal{L}_{\mathrm{i}k} u, \\ u(0) &= u(L), \\ u_\xi(0) &= u_\xi(L), \end{aligned} \tag{3.7}$$

with $\mathcal{L}_{\mathrm{i}k} : (H^2_{\mathrm{per}}(0, L))^2 \subset (L^2_{\mathrm{per}}(0, L))^2 \to (L^2_{\mathrm{per}}(0, L))^2$ defined by

$$\mathcal{L}_{\mathrm{i}k} := \begin{pmatrix} \gamma U_{\mathrm{per}}^{\gamma-1}\partial^2 + D_1 \cdot \partial - D_2 & -2U_{\mathrm{per}}V_{\mathrm{per}} \\ V_{\mathrm{per}}^2 & D\partial^2 + s\partial - [B - 2U_{\mathrm{per}}V_{\mathrm{per}}] \end{pmatrix}, \tag{3.8}$$

where $\partial := \partial_\xi + \mathrm{i}k$. We will occasionally refer to (3.7) as the dispersion relation for the linearization about u_{per}.

The operator $\mathcal{L}_{\mathrm{i}k}$ has compact resolvent for each k, so its spectrum consists of countably many isolated eigenvalues (Henry 1981). Since each of these eigenvalues is a root of the complex analytic dispersion relation $d(\lambda, \mathrm{i}k)$, one can continue the eigenvalues $\lambda_j(k)$, $j \in \mathbb{N}$ globally in k. By periodicity, each homotopy along $\lambda_j(k) \to \lambda_j(k + 2\pi)$ will map the set of eigenvalues $\lambda_j(k)$, $j \in \mathbb{N}$ onto itself (notice, however, that it will generally not be the case that each eigenvalue λ_j is mapped onto itself by the homotopy!). Therefore, the essential spectrum of the wave train u_{per} will generally consist of (at most) countably many connected components. One of these components is connected to the translational eigenvalue at the origin—see also Gardner (1993, 1997).

A spatially periodic pattern is *marginally stable* if its associated operator $\mathcal{L}_{\mathrm{i}k}$ and the dispersion relation $d(\lambda, \nu)$ (3.7) satisfy the conditions in Definition 1.

Each of the destabilization mechanisms through which a periodic pattern (U_{per}, V_{per}) may destabilize, is characterized by a specific configuration of the essential spectrum. The GKGS-model with $C \neq 0$ breaks the spatial symmetry that allows

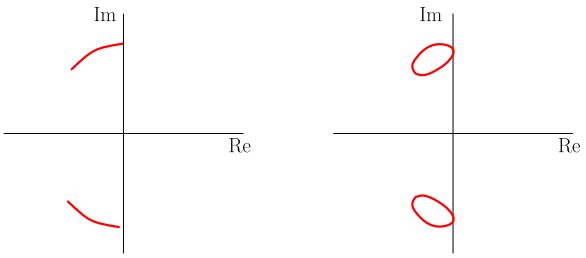

Fig. 7 Sketches of spectra at Hopf instabilities with $\lambda \in \mathbb{C}$. *Left*: Spectral branches for $C = 0$. Due to the reversibility, the spectral branches have collapsed to curved line segments (see Doelman et al. 2012). *Right*: Spectral branches for $C \neq 0$

for Turing patterns. This is a crucial observation, since the robust codimension-one destabilization mechanisms for generic wave trains are in principle different from the destabilization mechanisms for Turing patterns (Rademacher and Scheel 2007). We only discuss the robust codimension-one instability mechanisms that we have encountered for wave trains in our construction of Busse balloons for the GKGS-model; these are Turing–Hopf instability,[4] fold and sideband instability. Note that Hopf instabilities and sideband instabilities are robust destabilization mechanisms for all wave trains, while a fold is not a robust instability mechanism for generic spatially periodic patterns (with $\Omega \neq 0$ and $\kappa \neq 0$) though it is robust for Turing patterns ($\Omega = 0$) (see Rademacher and Scheel 2007).

A spatially periodic pattern u_{per} undergoes a Hopf instability at $A = A_*$ if the operator $\mathcal{L}_{\mathrm{i}k}$ in (3.8) is at marginal stability with $k_* \neq 0$ at critical eigenvalue $\lambda = \mathrm{i}\omega_*$ with $\omega_* \neq 0$. See Fig. 7. A fold and a sideband instability are both characterized as instabilities for which $k_* = 0$ at critical eigenvalue $\lambda = \mathrm{i}\omega_* = 0$. A sideband instability satisfies the additional condition that

$$\mathrm{Re}\,\frac{\partial^2 \lambda}{\partial k^2}\bigg|_{k=k_*} = 0. \tag{3.9}$$

We have depicted the difference between the fold (in the reversible case) and the sideband instability schematically in Fig. 8. Note that the dispersion relation in the reversible case possesses the symmetry $d(\lambda, \nu) = d(\lambda, -\nu)$ and is thus of the form

$$d(\lambda, \mathrm{i}k) = a_1\lambda + a_2\lambda^2 + a_3k^2 + a_4\lambda k^2 + a_5k^4 + \mathcal{O}\big(\lambda^3 + k^6\big), \tag{3.10}$$

where $a_j \in \mathbb{R}$. See also Rademacher and Scheel (2007). A fold occurs at $a_1 = 0$ and the sketches in the top row of Fig. 8 correspond to $a_1 < 0, a_1 = 0, a_1 > 0$ (and $a_j > 0$ for $j > 1$).

Methods and Implementation Notes For the construction of the Busse balloons, we have made use of the continuation and bifurcation software package AUTO (see Doedel 2007). The methods we have used to construct the Busse balloons are based upon Rademacher et al. (2007). In this section, we describe these methods.

[4] With slight abuse of terminology, in the context of perturbations of periodic patterns we abbreviate the Turing–Hopf instability to 'Hopf instability' in the rest of this paper.

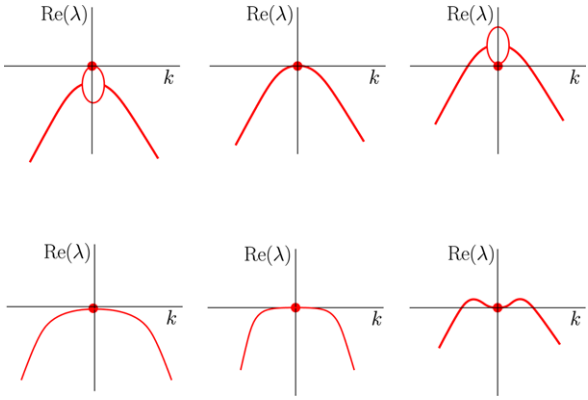

Fig. 8 Sketches of spectral configurations we encounter for wave trains close to marginal stability, when a system parameter is crossing a critical value. *Top row*: reversible fold for $C = 0$. *Bottom row*: sideband instability for general C

Using (3.2), a wave train solution (U, V) of the GKGS-model can be written as a first order system,

$$\begin{aligned} U_\xi &= P, \\ P_\xi &= -\frac{1}{\gamma U^{\gamma-1}}\big[\gamma(\gamma-1)U^{\gamma-2}P^2 + A(1-U) - UV^2 + (s+C)P\big], \\ V_\xi &= Q, \\ Q_\xi &= -D^{-1}\big[sQ - BV + UV^2\big]. \end{aligned} \tag{3.11}$$

We denote the vectorfield at the right hand of (3.11) by $F = F(U, P, V, Q) : \mathbb{R}^4 \to \mathbb{R}^4$ and write $\psi = (U, P, V, Q)^{\mathrm{T}}$. If we normalize the period L to unity, then (3.11) together with the boundary condition from (3.7) can be written as

$$\begin{aligned} \psi_\xi &= LF(\psi), \\ \psi(0) &= \psi(1). \end{aligned} \tag{3.12}$$

In AUTO, the nonlinear equation for the wave train (3.12) is solved together with the dispersion relation (3.7). By a translation of the independent variable via $\partial_\zeta = \partial_\xi + \mathrm{i}k$, the dispersion relation (3.7) can also be conveniently cast as a first order system. Translating back and normalizing the period L to unity again, one obtains

$$\begin{aligned} \phi_\xi &= L\big[\mathcal{A}_\lambda\big(u_{\mathrm{per}}(\xi)\big) - \mathrm{i}k\big]\phi, \\ \phi(0) &= \phi(1), \end{aligned} \tag{3.13}$$

with $\mathcal{A}_\lambda(u_{\mathrm{per}}(\xi))$ as in (3.4). Hence, we consider the boundary value problem

$$\begin{aligned} \psi_\xi &= LF(\psi), \\ \phi_\xi &= L\big[\mathcal{A}_\lambda\big(u_{\mathrm{per}}(\xi)\big) - \nu\big]\phi, \\ \phi(0) &= \phi(1), \\ \psi(0) &= \psi(1). \end{aligned} \tag{3.14}$$

In AUTO, we consider the boundary value problem (3.14) for general ν, as this allows us to switch between connected components of the essential spectrum (Rademacher et al. 2007). The essential spectrum is characterized by solutions to (3.14) such that $\nu = \mathrm{i}k$. We also impose the normalization conditions

$$\int_0^1 \langle \psi_\xi, \psi_{\text{old}} - \psi \rangle \, d\xi = 0; \qquad \int_0^1 \langle \phi_{\text{old}}, \phi \rangle \, d\xi = 1, \tag{3.15}$$

where the solutions ψ_{old} and ϕ_{old} are solutions from a previous continuation step or an initial solution (Rademacher et al. 2007).

Remark that $\psi \in \mathbb{R}^4$ and $\phi \in \mathbb{C}^4 \simeq \mathbb{R}^8$. Hence, we have $8+4 = 12$ real unknowns. On the other hand, we have 12 boundary conditions plus 3 real integral conditions, so we need $3 + 1 = 4$ parameters for continuation. We have at our disposal the system parameters A, B, C, and D, as well as $\operatorname{Re}\lambda$, $\operatorname{Im}\lambda$, the linear wavenumber $k = \operatorname{Re}\nu$, the imaginary part $\operatorname{Im}\nu$, the comoving frame speed s, and the spatial period L (which is related to the (nonlinear) wavenumber via $\kappa = \frac{2\pi}{L}$).

The sideband can be continued by defining the curvature

$$\lambda_{||} := \left. \frac{\partial^2 \operatorname{Re}\lambda_0}{\partial k^2} \right|_{k=k_*},$$

where $\lambda_0(k)$ is the curve through the origin, and k_* the wavenumber associated to $\lambda_0(k_*) = 0$ at the origin (cf. (3.9)). We refer to Rademacher et al. (2007) for an exact account on the implementation.

Hopf instabilities are continued in a similar way. Hopf instabilities generically occur when a connected component of the essential spectrum crosses the imaginary axis, see Fig. 7(b). A sufficient condition in order to fix the spectral component at marginal stability when a system parameter is changed, is

$$\operatorname{Re}\lambda|_{k=k_*} = 0 \quad \text{and} \quad \left. \frac{\partial \operatorname{Re}\lambda}{\partial k} \right|_{k=k_*} = 0, \tag{3.16}$$

This condition makes sure that the connected component of the essential spectrum extends into the left half-plane when continued from $\lambda(k_*) = \mathrm{i}\omega_*$. In AUTO, one therefore defines the tangency

$$\lambda_{|} := \frac{\partial \operatorname{Re}\lambda}{\partial k}$$

and keeps it zero during a continuation of Hopf instabilities, along with $\operatorname{Re}\lambda$. The implementation can be derived in the same way as for the sideband instability by differentiating the dispersion relation. (Note that some terms do not vanish for $\lambda \neq 0$.)

The above considerations are purely local in the spectrum. The determination of (marginal) stability requires more effort. We refer to Rademacher et al. (2007) for the algorithms. In addition, we checked the stability of the spectrum within the Busse balloon by explicit numerical evaluations on a grid.

3.1 The Existence Balloon

From Sect. 2.3 we know that the stationary state u_+ undergoes a Turing–Hopf instability at some $A = A_*$ with critical eigenmode e^{ik_*} and critical frequency $\lambda = i\omega_*$. Hence, at $A = A_*$ the dispersion relation of the stationary state u_+ (2.6) satisfies

$$d(i\omega_*, ik_*) = 0.$$

In Sect. 2.4 we deduced by our Ginzburg–Landau approach (see also Fig. 4) that for $A < A_{TH}$ sufficiently close to the Turing–Hopf instability of the background state $u_+ = (U_+, V_+)$, there exists a parabolically shaped region of periodic patterns. More precisely, for $A < A_{TH}$ sufficiently close to A_{TH}, there exists an interval $I_A = (\kappa_-(A), \kappa_+(A))$ such that for each $\kappa \in I_A$ there is a spatially periodic pattern with wavenumber κ and these form a continuous family. For each A, the endpoints $\kappa_\pm = \kappa_\pm(A)$ of the interval I_A are characterized by the dispersion relation of u_+ at A,

$$d(i\Omega_\pm, i\kappa_\pm) = 0. \tag{3.17}$$

We remark that this characterization for the endpoints $\kappa_\pm$ of I_A holds for a full range of $A < A_{TH}$ not necessarily close to A_{TH}. An equivalent formulation to (3.17) can be given by means of the first order ODE formulation of the linearization about u_+ (see (3.4)),

$$\phi_\xi = \mathcal{A}_\lambda(u_+)\phi \tag{3.18}$$

(notice that $\mathcal{A}_\lambda(u_+)$ is a constant matrix here). The dispersion relation (2.6) satisfies (3.17) for some Ω_* and κ_* if and only if there exists an Ω_* such that there is a solution to (3.18) for $\lambda = i\Omega_*$ that has purely imaginary eigenvalues $\nu = i\kappa_*$.

More generally, $\lambda \in \mathbb{C}$ is in the essential spectrum of u_+ if and only if there is a solution to (3.17) for some $\nu = i\kappa$. Since the wavenumbers ν from the dispersion relation of the stationary state u_+ (2.6) appear as eigenvalues to the spatial ODE (3.18), they are also referred to as spatial eigenvalues.

With AUTO, we have traced out a curve of boundary points $\kappa_\pm = \kappa_\pm(A)$ that mark the boundary of the existence balloon in (A, κ)-space. By construction, this provides an extension of the existence of the band of periodic patterns near the Turing–Hopf instability that is predicted by the GLE.

We digress a little on the characterization of the boundary of the existence balloon. Let $C \neq 0$, and consider fixed A and $\kappa_+ = \kappa_+(A)$, so that there exists a $\lambda = i\Omega$ such that (3.18) has purely imaginary spatial eigenvalue κ_+ and therefore a pair of complex conjugated spatial eigenvalues $\pm\kappa_+$. Hence, for fixed A, and by changing the speed s of the comoving frame, typically two spatial eigenvalues $\pm i\kappa_+$ cross the imaginary axis so that a Hopf bifurcation occurs. Therefore, locally there exists a one-parameter family of periodic orbits parametrized by the speed s.

Likewise, there exists a one-parameter family of periodic orbits when the other pair of eigenvalues $\pm\kappa_-$ crosses the imaginary axis. By a continuation of the two families of periodic patterns with AUTO, we have found that they are connected. See Fig. 9(b). This extends the band of periodic patterns that is described by the GLE close to the Turing–Hopf bifurcation for $A = A_{TH}$.

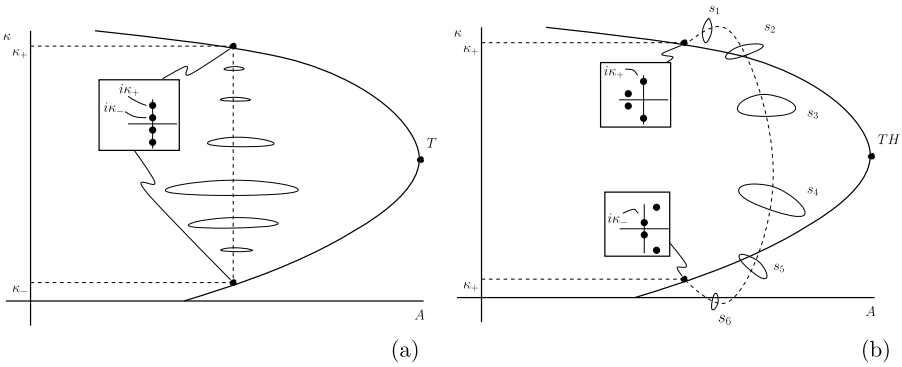

Fig. 9 The boundary of the existence region near the Turing and Turing–Hopf bifurcations. *Closed curves* are sketches of some periodic patterns *for fixed* A, illustrating the amplitude variations. Compare with Fig. 4. *Insets* show the configurations of spatial eigenvalues of u_+ at the boundary of the existence balloon at this value of A. (**a**) The reversibly symmetric case $C = 0$ with $s \equiv 0$; spatial eigenvalues are two pairs of purely imaginary values. (**b**) Asymmetric case $C, s \neq 0$, where spatial eigenvalues change with s; note that at each end of the *dotted curve*, a different (single) pair of eigen values lies on the imaginary axis

If $C = 0$, the reversible symmetry forces the spatial spectrum to be symmetric with respect to the real axis and the imaginary axis. At the Turing bifurcation of the stationary state u_+, the spatial spectrum shows a 1:1 reversible Hopf bifurcation: there are two identical pairs of complex conjugate purely imaginary spatial eigenvalues $\pm k_*$. By the reversible symmetry, for $A < A_{\mathrm{TH}}$, two pairs of spatial eigenvalues will move along the imaginary axis. Then one can apply the reversible Lyapunov center theorem (Devaney 1976): for (non-resonant) κ_- as well as for (non-resonant) κ_+, there is a one-parameter family of periodic orbits with limiting wavenumber $\kappa_\pm$ as the orbits approach the background state u_+. (At resonances additional bifurcations occur, which are not relevant here.) Again, by continuation, we find that the family that emerges from κ_- is connected to the family that emerges from κ_+, which in turn extends the connected band of periodic solutions close to the Turing–Hopf bifurcation that we know from the Ginzburg–Landau analysis. See Fig. 9(a).

The spectral stability of a stationary state is partly characterized by its spatial spectrum. In Fig. 10 we have plotted the spatial spectrum of the stationary states u_+ and u_- for different values of either A and the comoving frame speed s. We briefly comment on Fig. 10(b) here. First, we check that the speed of the critical pattern that appears at the Turing–Hopf instability equals $s_* = -\frac{\omega_*}{k_*}$. If we write the (stationary) dispersion relation $d_s(\lambda, \nu)$ in (2.6) with respect to a comoving coordinate $\xi = x - st$, we have $d_s(\lambda, \nu) = d_0(\lambda - s\nu, \nu)$. In particular, if $k_* \neq 0$ we see

$$d_{\omega_*/k_*}(0, \mathrm{i}k_*) = d_0(\mathrm{i}\omega_*, \mathrm{i}k_*) = 0.$$

Secondly, the spatial spectrum of the fold of the stationary states u_- and u_+ is characterized by a complex conjugated pair of purely imaginary eigenvalues that come together in the origin and move on to the real axis. Thirdly, we remark that for fixed $A_{\mathrm{SN}} < A < A_{\mathrm{TH}}$ for any relevant value of s and $\kappa_-(A) < \kappa < \kappa_+(A)$, the spatial spectrum of the stationary state u_+ has no intersection with the imaginary axis. In

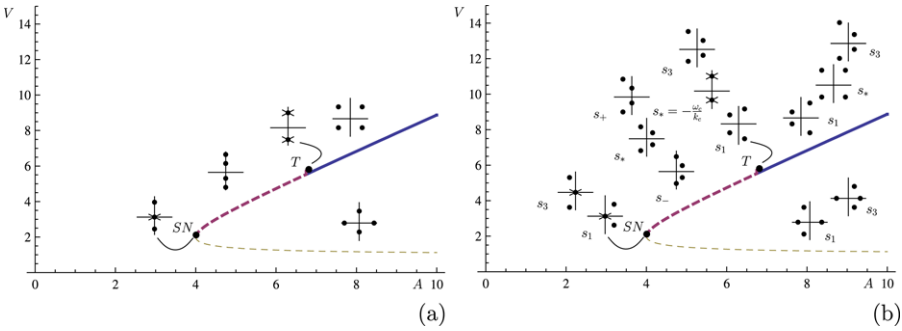

Fig. 10 The $V_{\pm}$-component of the stationary states $u_{\pm}$ against A, with $B = 1$. (**a**) Reflection symmetric case $C = 0$. (**b**) The nonsymmetric case $C \neq 0$. The *insets* show the typical configuration of the spatial spectrum of the stationary state u_+. In the nonsymmetric case, the spatial spectrum depends on s—the speed of the pattern—and thus various distinct configurations have been plotted. Compare to Fig. 9

Fig. 10(b), s_+ is the critical frame speed when κ_+ crosses the imaginary axis and s_- is the critical frame speed when κ_- crosses the imaginary axis. In the pictures of spatial spectra for the different s_i, $i = 1, 2, 3$, it is understood that the comoving frame speed s varies but differs from either s_-, s_+ or s_*.

3.2 Busse Balloons for the GKGS-Model

In this section we present a series of Busse balloons for a number of parameter sets that we have constructed using AUTO (by methods discussed above).

In Klausmeier (1999) the parameters of the Klausmeier model have been estimated. In our scaling of the GKGS-model, it is estimated that $A_{\text{tree}} \in [18.9, 169]$, $B_{\text{tree}} \in [5.7 \times 10^{-3}, 5.1 \times 10^{-2}]$ and $D_{\text{tree}} \in [4.2 \times 10^{-4}, 1.2 \times 10^{-2}]$ and that $A_{\text{grass}} \in [0.127, 1.13]$, $B_{\text{grass}} \in [5.7 \times 10^{-2}, 5.1 \times 10^{-1}]$ and $D_{\text{grass}} \in [5.2 \times 10^{-3}, 1.5 \times 10^{-2}]$. The advection term that measures the slope of the surface has been put to $C = 182.5$. We therefore set $B = B_{\text{grass}} = 0.2$ and $D = 1.0 \times 10^{-3}$. In the results we are about to present, we found interesting behavior for C satisfying $0 < C < 1$, which is relatively small compared to the estimate of C in Klausmeier (1999). There seem to be no significant changes in the characteristics of the Busse balloon for $C > 1$. Therefore, we focus on Busse balloons with these parameter values for C rather than on Busse balloons with $C \approx 182.5$. This means that we focus on a presentation of Busse balloons that describe periodic patterns for ecosystems with a weaker slope than in Klausmeier (1999). The power γ in the nonlinear diffusion term is either set to $\gamma = 1$ or to $\gamma = 2$.

We checked that the Turing–Hopf bifurcation indeed takes place at the parameter values predicted by the analysis in Sect. 2.2 and 2.3. Consider for instance Fig. 11. There, $B = 0.2$, $C = 0.4$, $D = 0.001$, $\gamma = 1$ and further $A_{\text{TH}} \approx 1.24$ and $k_* \approx 9.1$. The estimates for a_* and k_* from Proposition 2 are satisfied given that $(2\gamma + 1)\beta - (\gamma + 1)\alpha = 2\sigma$. Further, it must hold that ν satisfies its critical scaling (2.18): $\nu = \frac{1}{2}(3 - \gamma)\alpha + (\gamma - 2)\beta$. For $\alpha = \frac{1}{2}$, $\beta = 1$, $\gamma = 1$, $\nu = -\frac{1}{2}$ and $\sigma = 1$ (so that $D = 0.001$ gives $\delta = \sqrt{0.001}$) these conditions are satisfied. The rescaling

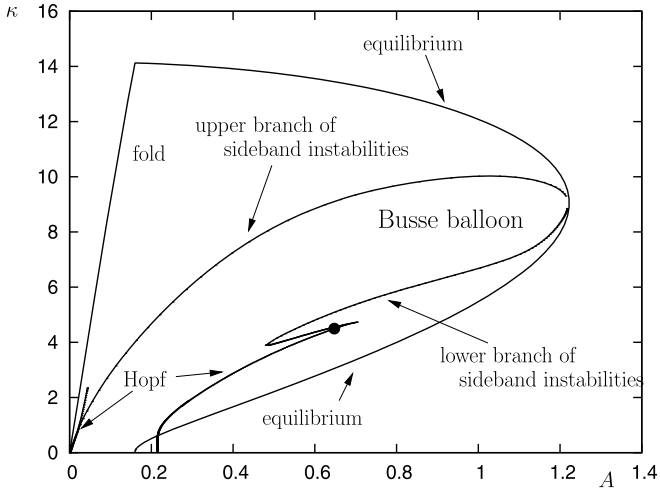

Fig. 11 Busse balloon and existence balloon for $B = 0.2$, $C = 0.4$, $\gamma = 1$. Here, periodic patterns become unstable by either sideband or Hopf instability. Compare Fig. 2

for k introduced in Sect. 2.3 is then $k_* = \delta^{\frac{1}{2}(\gamma+1)\alpha-\gamma\beta}\tilde{k}_* = 1.62$ since $\tilde{k} \approx 9.0$. Further, we compute $a_* = A\delta^{-\alpha} = 1.24 \cdot \delta^{-1/2} = 7.0$, $b = B\delta^{-\beta} = 0.2 \cdot \delta^{-1} = 6.3$ and $c = C\delta^{-\nu} = 0.4 \cdot \delta^{1/2} = 0.07$. Hence, the estimates of Proposition 2 are easily verified: $k_*^2 = 1.62^2 < 6.3 = b$ and $a_*^2 = 7.0^2 > 42.9 \approx (3 - 2\sqrt{2}) \cdot 6.3^3$.

Both branches of sideband instabilities extend far into the region that is not asymptotically close to A_{TH}. More precisely, there exists an interval $I_{\mathrm{sb}} = (A_{\mathrm{sb}}, A_{\mathrm{TH}})$ such that for each $A \in I_{\mathrm{sb}}$ there is an interval $(\kappa_{\mathrm{sb}-}(A), \kappa_{\mathrm{sb}+}(A))$ of stable patterns that destabilize by sideband instabilities at $\kappa_{\mathrm{sb}-}(A)$ and $\kappa_{\mathrm{sb}+}(A)$. Notice that this is analogous to the existence of the Eckhaus region of stable patterns near A_{TH} (see Fig. 4).

3.2.1 Hopf Instabilities

In Fig. 11 both branches of sideband instabilities are crossed by a branch of Hopf instabilities. The nature of these Hopf instabilities can be better understood if we first deal with the situation for $C = 0$, so we first discuss the Hopf instabilities for $C = 0$ and refer to the more elaborate account on this topic in Doelman et al. (2012) when necessary.

For $C = 0$, the branch of Hopf instabilities decouples in two intertwining curves of Hopf bifurcations (see Doelman et al. 2012). As is shown in Doelman et al. (2012), the reversibility induces a symmetry of the essential spectrum Σ_{ess}. See, for example, Fig. 7. Each connected component that has the structure of a closed loop for $C > 0$, collapses to a (slightly) bended line-segment in the limit $C = 0$. Due to an additional effect (called the 'Belly dance', see Doelman et al. 2012), a Hopf instability occurs only if one of the end points of the destabilizing line segment crosses the imaginary axis (see Fig. 7(b)). It is shown that the end points are associated with Floquet multipliers $m = \mathrm{e}^{\mathrm{i}k \cdot \frac{2\pi}{L}}$ that satisfy $m = -1$ or $m = 1$. Hence, the Hopf bifurcation for $C = 0$ occurs either with respect to a Fourier mode that is in phase ($m = 1$) with the

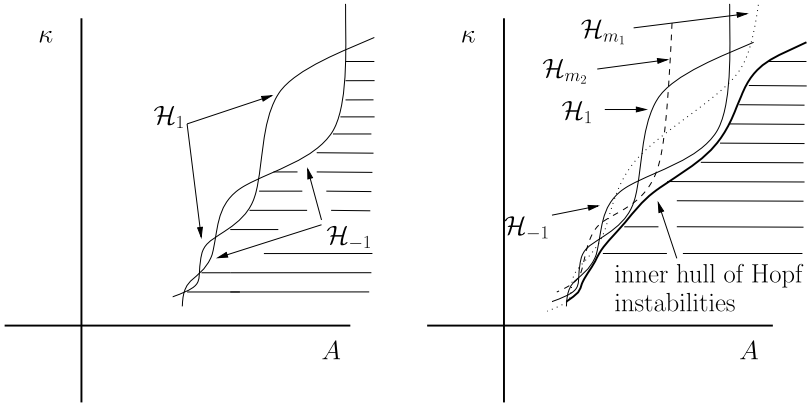

Fig. 12 *Left*: sketch of a Hopf dance for the GKGS-model with $C = 0$. *Right*: four Hopf curves, each associated to a different Floquet multiplier m. For each $m \in \mathbb{S}^1$ there exists a Hopf curve $\mathcal{H}_m$. At the *right*, the inner hull of Hopf instabilities forms the boundary of the Busse balloon. It is assumed that $m_1 \neq m_2$ and $m_1, m_2 \neq \pm 1$. The *horizontal lines* indicate the stable region

destabilizing periodic pattern or with respect to a Fourier mode that is exactly out of phase ($m = -1$) with the destabilizing pattern. Each of these instabilities traces out a different curve in (A, κ)-space. As a consequence, in the reversible case the boundary of the Busse balloon associated to a Hopf bifurcation, typically has a (non-smooth) fine structure of two intersecting curves, one associated to $m = 1$ and the other to $m = -1$, separated by co-dimension two points; the intersections of these $m = \pm 1$ curves.

For $C > 0$, the reversible symmetry is broken. Therefore, the essential spectrum consists of at most countably many open or closed loops. Each loop is parametrized by Floquet exponents k, $k \in [0, L]$, or equivalently, by Floquet multipliers $m \in \mathbb{S}^1$. A Hopf instability occurs when a loop crosses the imaginary axis. In Fig. 7(a) one observes a closed loop of essential spectrum crossing the imaginary axis. The destabilizing Fourier mode is characterized by its Floquet multiplier $m \in \mathbb{S}^1$. The difference between the reversible case and the irreversible case is that in the irreversible case the destabilizing modes exhaust all Floquet multipliers $m \in \mathbb{S}^1$, while in the reversible case the destabilizing Floquet multiplier is either $m = -1$ or $m = 1$. For each Floquet multiplier $m \in \mathbb{S}^1$ there exists a curve of Hopf instabilities that is associated to m. The multitude of these curves defines an inner hull of Hopf instabilities that is the boundary of the Busse balloon. See Fig. 12 for a schematic picture.

3.2.2 The Homoclinic Fall of Patterns

An intriguing characteristic of all Busse balloons we have constructed for the GKGS-equation is that the homoclinic pattern, i.e., a localized vegetated 'oasis' state with wavenumber $\kappa = 0$, is the last pattern to become unstable if we change A and keep all other parameters fixed. On the one hand, this is not atypical for reaction–diffusion models; in the context of Gierer–Meinhardt type equations it is called Ni's conjecture (see Ni 1998 and Doelman et al. 2012 for a more thorough discussion). On the other

hand, it is certainly not well understood why this 'homoclinic fall of patterns' turns up naturally in reaction–diffusion equations.

The homoclinic fall of (stable) patterns is strongly associated to the appearance of the 'Hopf-dance' at the boundary of the Busse balloon near the homoclinic tip that we described in Sect. 3.2.1. In fact, the Hopf-dance phenomenon has been discovered in the context of our research of the GKGS model and led to Doelman et al. (2012) as 'spin-off'. In this paper it is shown for a class of reversible model problems that the intertwining $m = \pm 1$ Hopf curves described above (Sect. 3.2.1) accumulate on the homoclinic tip of the Busse balloon as A approaches its minimal value (for which stable periodic patterns exist). Thus, the curves have countably many intersections that accumulate on the homoclinic tip of the Busse balloon—see Fig. 12(a) for a schematic sketch. The GKGS-model is not of this class (certainly not for $\gamma = 2$) but we found that all Busse balloons for the GKGS model with $C = 0$ do exhibit this 'Hopf-dance' near the homoclinic tip. Of course, this fine structure and its associated co-dimension two points immediately disappear as C becomes unequal to zero and gives rise to a simple smooth oscillating curve of Hopf instabilities. See Fig. 12.

3.2.3 Upper Branch of Sideband Instabilities

An intriguing phenomenon is the fact that this branch of Hopf instabilities crosses the upper branch of sideband instabilities, moves out of the Busse balloon for increasing C. See Fig. 13 for a series of (zoomed in) Busse balloons and a schematic sketch from which the 'dynamics' of the Hopf bifurcation curve are more clear. More precisely, there exists a $C_{\mathrm{T}_1} > 0$ such that the branch of Hopf instabilities is tangent to the branch of sideband instabilities. For C slightly larger than C_{T_1}, two connected components of the boundary of the Busse balloon consist of Hopf instabilities. At $C = C_{\mathrm{H}} > C_{\mathrm{T}_1}$ the branch of Hopf instabilities gets connected to the origin. For C slightly larger than C_{H}, locally there is only one connected component of the boundary of the Busse balloon that consists of Hopf instabilities. If one increases C even further, it passes a second value C_{T_2} at which there is a tangency between the branch of Hopf instabilities and the branch of sideband instabilities. For $C > C_{\mathrm{T}_2}$ the sideband is the only destabilization mechanism for long wavelength patterns.

If $C = 0$, the sideband reaches the A-axis at $A \neq 0$. However, the intersection of the upper branch of sideband instabilities with the A-axis rapidly moves to $A = 0$ as C is increased. This is certainly not fully understood.

3.2.4 Lower Branch of Sideband Instabilities

We recall that the lower branch of sideband instabilities is intersected by a branch of Hopf instabilities as well. See Fig. 14, where we have magnified the intersection between the lower branch of sideband instabilities and the right branch of Hopf instabilities. It is visible as a strikingly sharp cusp. In Fig. 14 we have also depicted the spectrum associated to the stability of a solution at the sideband instability close to the crossing point, denoted by ①, the spectrum associated to the solution at the crossing point, denoted by ②, and the spectrum associated to a solution close to the crossing point undergoing a Hopf instability, denoted by ③. The crossing point ② is

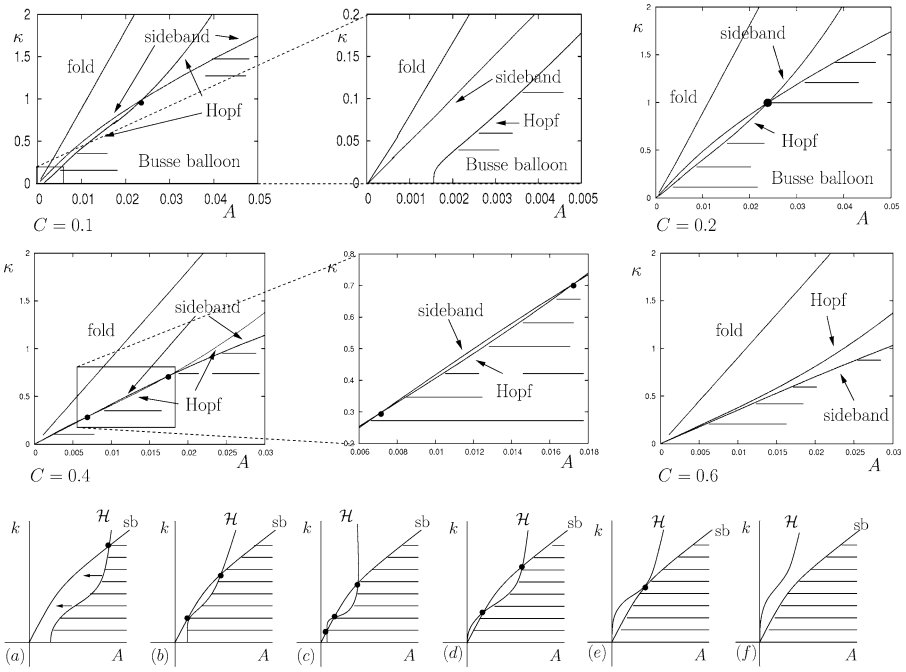

Fig. 13 *Upper panels*: The *left* Hopf curve moving out of the Busse balloon for increasing C. The *horizontal lines* indicate the stable region. *Center panel* magnify the *box* in *left panels*. The *fold curve* in the *upper left panel* has not been plotted in the other panels for readability. *Lower panels*: A schematic sketch of the same process (sb = sideband). (**a**) The curve of Hopf instabilities has one intersection with the upper branch of sideband instabilities. (**b**) At $C = C_{T_1}$, there is a tangency between the two curves. (**c**) For $C_{T_1} < C < C_H$ there are two connected components of the boundary of the Busse balloon formed by Hopf instabilities. (**d**) At $C = C_H$, the curve of Hopf instabilities is connected to the origin: only one connected component of the boundary that consists of Hopf instabilities. (**e**) At $C = C_{T_2}$, there is a second tangency between the two curves remains. (**f**) For $C > C_{T_2}$, the sideband remains as the only destabilization mechanism in the homoclinic tip (see Sect. 3.2.2)

a codimension-two point at the boundary of the Busse balloon: the solution at the crossing point simultaneously undergoes a sideband instability and Hopf instability, as is visible in the plot of the spectrum of solution 2.

When C approaches zero, the lower branch of sideband instabilities stretches out towards the A-axis and thereby decreases the size of the branch of Hopf instabilities. The Hopf instabilities disappear at $C = 0$ where also the sideband curve merges with the very nearby fold curve (see Doelman et al. 2012). The fact that reversible folds yield sideband instabilities upon symmetry breaking can be readily seen by perturbing (3.10). See also Fig. 8. In Figs. 15 we have plotted three close-ups of the Busse balloons for $C = 0.1$, $C = 0.01$, and $C = 0.001$.

A second intriguing phenomenon is the irregular 'jazzy' behavior of the lower branch of sideband instabilities for relatively small C ($C = 0$ to approximately $C = 0.8$). See Fig. 16. This fine structure of the lower branch of sideband instabilities is in sharp contrast with the regular, parabolically shaped Eckhaus region for A near A_{TH}.

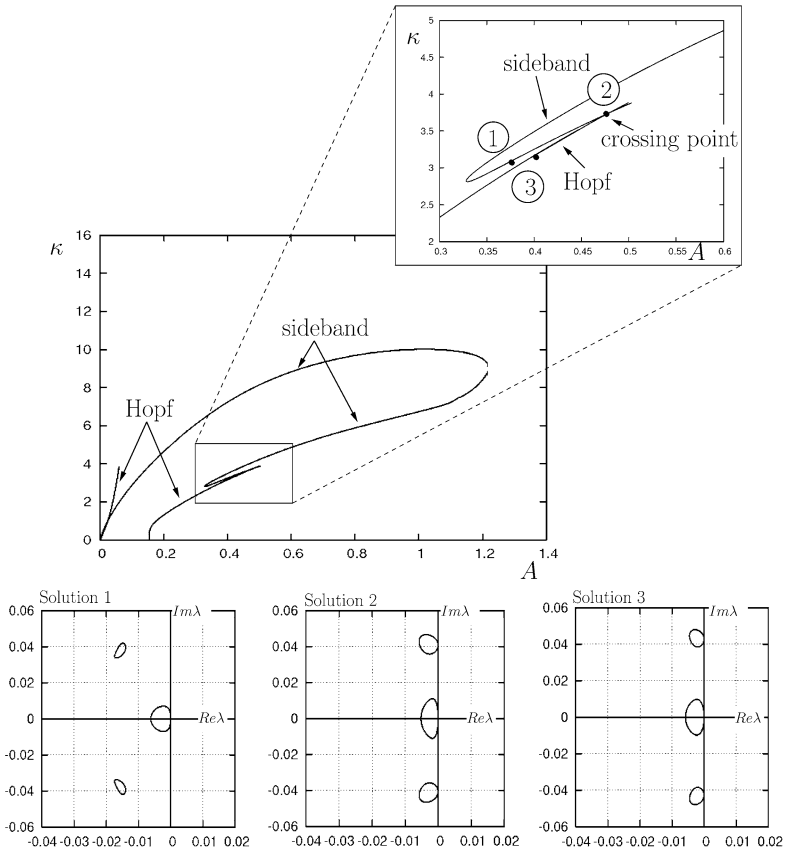

Fig. 14 Close-up of the crossing point between the *right curve* of Hopf instabilities and the *lower branch* of sideband instabilities. Here, $C = 0.2$ and $B = 0.2$. The spectra near the origin for the solutions 1, 2 and 3 indicated in the magnification are plotted in the *three figures* at the *bottom*

Even a closed curve of sideband instabilities occurs (see Fig. 16(b)). For increasing C, the fine structure gradually disappears.

While the fine structure of sideband instabilities lies in the unstable region, we digress a little on its structure and location within the existence region. To the right of the fine structure lies the fold curve mentioned above (see Fig. 15, left), which we refer to as the *right fold*. For the C values considered in Fig. 16, the right fold curve (see the discussion in Sect. 3.1) terminates on the equilibrium curve at some $(A_{\mathrm{fe}}, \kappa_{\mathrm{fe}})$ near $(0.8, 4)$. Hence, for $A < A_{\mathrm{fe}}$ there is a second co-existing 'sheet' of (unstable) spatially periodic patterns.

In the lower panel of Fig. 17(a) we plot (for a different C) the L^2-norm for fixed κ to illustrate the different sheets of solutions. Here the co-existence region is rather small. See top right panel. continuation of periodic patterns for constant wavenumber κ. Comparison with Figs. 15 and 16 shows how the fine structure of sideband instabilities is to the left of the right fold, thus lying on the same "sheet" of solutions as the stable periodic patterns of the Busse balloon.

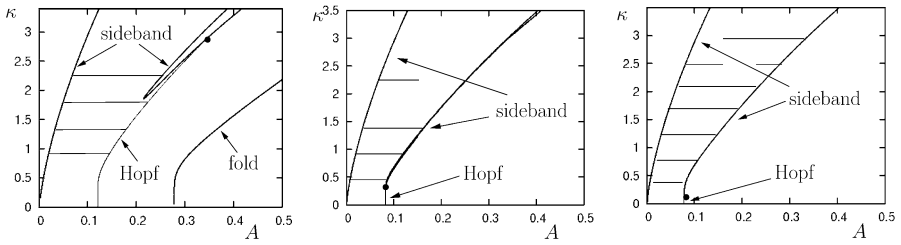

Fig. 15 The *right branch* of Hopf instabilities disappears into the A-axis when $C \downarrow 0$. At the *left*, we see a part of the Busse balloon for $C = 0.1$. In the *middle*, $C = 0.01$. At the *right*, $C = 0.001$. The *fold curve* plotted in the *left panel* has moved very close to the Hopf and sideband curves in the other panels, so that it cannot be visually distinguished

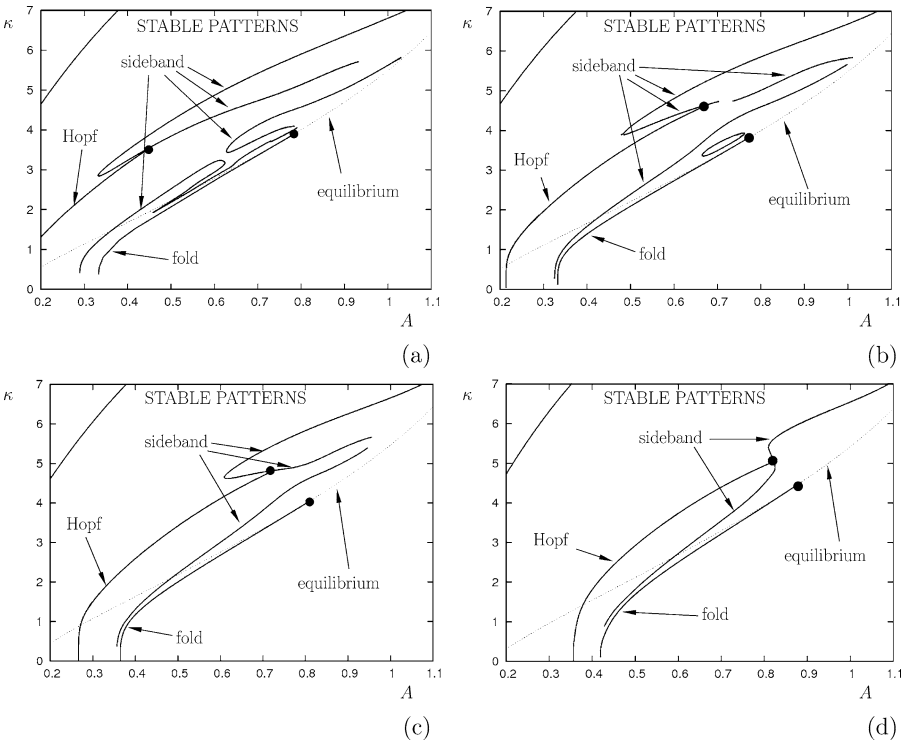

Fig. 16 (**a**)–(**d**) The fine structure of the lower branch of sideband instabilities for $B = 0.2$ and (**a**) $C = 0.2$, (**b**) $C = 0.4$, (**c**) $C = 0.6$, and (**d**) $C = 1.0$. The equilibrium continues through the fold and reaches a second sheet of (unstable) patterns; therefore it is plotted with a *dashed curve*. The intersection point of the Hopf instabilities with the sideband is indicated with a *black circle*. Also, the intersection point of the fold with the equilibrium is indicated with a *black circle*. Note that some pieces of the curve of sideband instabilities are missing; here the continuation of the sideband with AUTO becomes extremely difficult since the norm of one of the eigenvectors in (3.15) rapidly increases

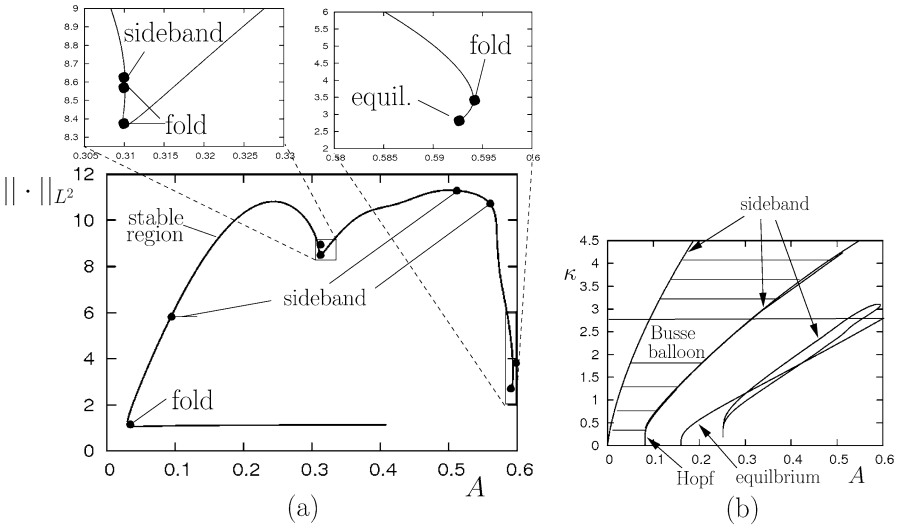

Fig. 17 Computations for $B = 0.2$, $C = 0.01$. (**a**) Plot for continuation in A with constant wavenumber $\kappa = 2.78$. *Top panels* magnify the indicated regions. (**b**) Part of the existence balloon. The *thick line* indicates the value of κ used in (**a**)

An additional phenomenon of the existence region is shown by the region near $A = 0.3$: there are two more folds which emerged through a cusp bifurcation when decreasing C from $C = 0.2$. lower branch, thereby giving rise to a cusp. We notice that this behavior of the unstable sheet of solutions close to the Busse balloon is highly nongeneric. Indeed, the existence region has a much richer structure than what we encounter within the Busse balloon. Finding out the precise geometrical mechanism that triggers the formation of this cusp is beyond the scope of the present paper. However, this will be the subject of future research.

3.3 Busse Balloons for $C > 0$ and $\gamma = 2$

We are not aware of any (even partial) representations of a Busse balloon for a system with nonlinear diffusion in the literature. Nevertheless, the approach with AUTO developed here can also be directly applied to the GKGS model (1.5) with $\gamma > 1$. In Fig. 18 an existence and a Busse balloon for periodic patterns of the GKGS-model with $\gamma = 2$ and $B = C = 0.2$ are shown. One can see that the structure of the Busse balloon of the existence region closely resembles the structure of the Busse balloon and existence region of the GKGS-model for $\gamma = 1$ (see for instance Fig. 11).

As before for $\gamma = 1$, we check that the Turing–Hopf bifurcation indeed takes place at the parameter values predicted by the analysis in Sects. 2.2 and 2.3. We therefore check whether $k_*^2 < b$ and $a_*^3 = a_*^{\gamma+1} > g\gamma b^{2\gamma+1} = 2gb^5$ with $k = k_*$ scaled as in Sect. 2.3 and Fig. 18. There, $B = 0.2$, $D = 0.001$, $\gamma = 2$, and further $A_{\mathrm{TH}} \approx 0.525$ and $k_* \approx 8.9$. If $\gamma = 2$, the estimates for a_* and k_* from Proposition 2 are satisfied given that $5\beta - 3\alpha = 2\sigma$. Since $D = \delta^{2\sigma} = 0.001$, we choose $\sigma = 1$ and $\delta = \sqrt{0.001}$ and $\alpha = \beta = \sigma = 1$. The rescaling for k introduced in

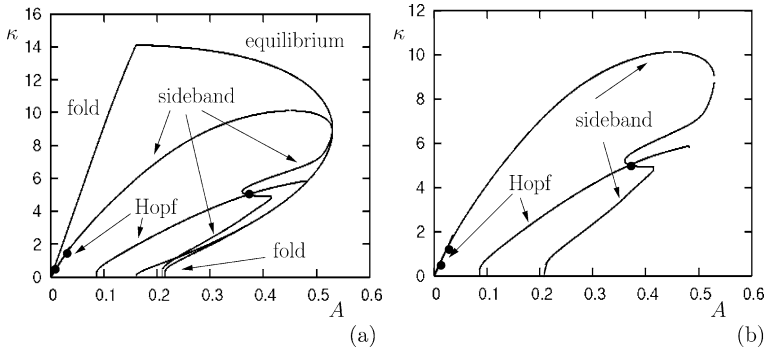

Fig. 18 An existence balloon (*left*) and a Busse balloon (*right*) for the GKGS-model with $\gamma = 2$. B and C are $B = C = 0.2$. The intersection points of the Hopf instabilities with the upper and lower curves of sideband instabilities are indicated with a *black circle*

Sect. 2.3 is then $\tilde{k}_* = \delta^{-\frac{1}{2}(\gamma+1)\alpha+\gamma\beta} k_* = \delta^{1/2} k_* = (0.001)^{1/4} \cdot 8.9 \approx 1.58$. Further, we compute $a = A\delta^{-\alpha} = 0.525 \cdot \sqrt{1000} \approx 16.6$ and $b = B\delta^{-\beta} = 0.2 \cdot \sqrt{1000} \approx 6.3$. Hence, the estimates of Proposition 2 are verified by $k_*^2 = 1.58^2 < 6.3 = b$ and $a_*^3 = 16.6^3 \approx 4.75 \times 10^3 > 3.47 \times 10^3 \approx 2gb^5$.

A priori, the GKGS-model for $\gamma = 2$ can of course not be interpreted as a 'perturbation' of the GKGS-model for $\gamma = 1$. Quantitatively the structure between the Busse balloon for $\gamma = 2$ and the Busse balloons for $\gamma = 1$ is quite different. This is already apparent in the simple verification of the parameter estimates for a, b, and c above. Nevertheless, qualitatively the structure of the Busse balloon for $\gamma = 2$ is remarkable akin to the structure of the Busse balloons for $\gamma = 1$. All main features of the (behavior of the) Busse balloon for various C as studied in the previous section for $\gamma = 1$ and described in the Introduction, also appear for $\gamma = 2$. Figure 18 shows that the sideband instabilities make most of the boundary of the Busse balloon, until the upper and lower branches of sideband instabilities are crossed transversally by Hopf instabilities for decreasing wavenumbers k. Also, for relatively small $C > 0$ there is a 'Hopf dance' (if $C = 0$) in the homoclinic tip of the upper branch of sideband instabilities. In the figure, where $C = 0.2$, there is a Hopf curve crossing the upper branch of sideband instabilities. Just as in the case for $\gamma = 1$, the left curve of Hopf instabilities disappears into the unstable region for bigger values of C. These are not new phenomena and are known from the previous numerical analysis of the GKGS-model for $\gamma = 1$.

Acknowledgements The authors thank Max Rietkerk for sharing his insights and the stimulating discussions.

Appendix: Derivation of the Ginzburg–Landau Equation

In this appendix, we outline the derivation of the Ginzburg–Landau equation for the amplitude $\mathcal{A}$ of the pattern that appears at the Turing–Hopf bifurcation. Each of the four different cases of Fig. 1 can be derived from the expressions given in this appendix by considering either $\gamma = 1$ or $c = 0$, or both.

In Appendix A.1 we derive the Ginzburg–Landau equation for the special case that $\gamma = 1$ and $c = \sqrt{\frac{2}{3}b}$ that was presented in Sect. 2.5.3.

The Ginzburg–Landau Ansatz for patterns that emerge at the Turing–Hopf instability can, for the rescaled GKGS-system (2.38), be written as

$$\begin{aligned}\begin{pmatrix} U \\ V \end{pmatrix} = \mathcal{A}\begin{pmatrix} 2b \\ \eta_{\gamma,c} \end{pmatrix} e^{i(k_* x + \omega_* t)} &+ \varepsilon \begin{pmatrix} X_{02} \\ Y_{02} \end{pmatrix} + \cdots \\ &+ \varepsilon \begin{pmatrix} X_{12} \\ Y_{12} \end{pmatrix} e^{i(k_* x + \omega_* t)} + \varepsilon^2 \begin{pmatrix} X_{22} \\ Y_{22} \end{pmatrix} e^{2i(k_* x + \omega_* t)} + \text{c.c.} + \cdots \\ &+ \varepsilon \begin{pmatrix} X_{13} \\ Y_{13} \end{pmatrix} e^{i(k_* x + \omega_* t)} + \text{c.c.} + \cdots, \end{aligned} \tag{A.1}$$

where $\mathcal{A}$ and X_{ij} are functions of $\xi = \varepsilon x$ and $\tau = \varepsilon^2(x - c_g t)$ and c_g the group velocity defined by (2.26). Substituting this expansion in the GKGS-system (2.38) and collecting terms of equal powers of ε and the Fourier modes $e^{i(k_* x + \omega_* t)}$, we derive expressions for $X_{02,12,22,13}$ and $Y_{02,12,22,13}$ subsequently. Notice that the scaling in (2.38) has the advantage that the terms of order ε^2 only play a role in the equations for X_{13} and Y_{13}.

As mentioned in paragraph 2.4, the solvability condition can be applied to solve an equation of the form

$$\mathcal{M}_{i\omega_*}(a_*, k_*, c)x = y. \tag{A.2}$$

The equations for X_{1j}, Y_{1j}, $j = 2, 3$ are of this form, with

$$\mathcal{M}_{i\omega_*}(a_*, k_*, c) = \begin{pmatrix} -\Gamma k_*^2 - \frac{a_*^2}{b^2} + ick_* & -2b \\ \frac{a_*^2}{b^2} & -k_*^2 + b - i\omega_* \end{pmatrix}. \tag{A.3}$$

We briefly point out the construction of the set of solutions for (A.2). The construction for $c = 0$ differs from that for $c \neq 0$.

If $c \neq 0$, the matrix in (A.3) has two eigenvalues, $\lambda_+ = 0$ and

$$\lambda_- = -\Gamma k_*^2 - \frac{a_*^2}{b^2} + ick_* - k_*^2 + b - i\omega_*. \tag{A.4}$$

If $y \in \text{Rg}\,\mathcal{M}_{i\omega_*}(a_*, k_*, c)$ and $c \neq 0$, the set of solutions to (A.2) is given by

$$x = \frac{1}{\lambda_-} y + \ker \mathcal{M}_{i\omega_*}(a_*, k_*, c).$$

On the other hand, if $c = 0$, we know from Proposition 1 that

$$a_*^{\gamma+1} = \gamma g b^{2\gamma+1} \quad \text{and} \quad k_*^2 = \frac{1}{2}(1 - g).$$

It is then straightforward to show that

$$\mathcal{M}_{\mathrm{i}\omega_*}(a_*,k_*,0)=\begin{pmatrix}-\frac{1}{2}(g-7)(\frac{g\gamma}{b})^{\frac{2}{\gamma+1}}b^2 & -2b\\ (\frac{g\gamma}{b})^{\frac{2}{\gamma+1}}b^2 & \frac{1}{2}b(1+g)\end{pmatrix} \tag{A.5}$$

and that $\lambda_-=0$ if $\gamma=1$. It is also straightforward to show that both columns of $\mathcal{M}_{\mathrm{i}\omega_*}(a_*,k_*,0)$ span the range. We call the second column v_1. So if y from (A.2) lies in the range, there exists an $\alpha\in\mathbb{R}$ such that $y=\alpha v_1$. Hence, if $c=0$, the set of solutions to (A.2) can be presented as

$$x=\alpha\cdot\begin{pmatrix}0\\1\end{pmatrix}+\ker\mathcal{M}_{\mathrm{i}\omega_*}(a_*,k_*,0). \tag{A.6}$$

By plugging in the expansion (A.1) into (2.38) one obtains at order $\mathcal{O}(\varepsilon)$ an equation for $(X_{02},Y_{02})^{\mathrm{T}}$,

$$\begin{pmatrix}X_{02}\\Y_{02}\end{pmatrix}=\left[-2\frac{b^4}{a_*^3}|\eta_{\gamma,c}|^2-8\frac{b^2}{a_*}\operatorname{Re}(\eta_{\gamma,c})\right]\begin{pmatrix}1\\0\end{pmatrix}|\mathcal{A}^2|. \tag{A.7}$$

We use shorthands x_{02}, y_{02} for $X_{02}=x_{02}|\mathcal{A}|^2$, $Y_{02}=y_{02}|\mathcal{A}|^2$. The values for x_{02} and y_{02} can be read from (A.7). At order $\mathcal{O}(\varepsilon E)$, we find equations of the form

$$\mathcal{M}_{\mathrm{i}\omega_*}(a_*,k_*,c)\begin{pmatrix}X_{12}\\Y_{12}\end{pmatrix}=\begin{pmatrix}x_{12}\\y_{12}\end{pmatrix}\mathcal{A}_\xi$$

which can be solved if $(x_{1j},y_{1j})^{\mathrm{T}}\in\operatorname{Rg}\mathcal{M}_{\mathrm{i}\omega_*}(a_*,k_*,c)$. We find

$$\begin{aligned}x_{12}&=[-4b\mathrm{i}\Gamma k_*-2bc]/\lambda_-;\\ y_{12}&=[-\eta_{\gamma,c}c_{\mathrm{g}}-2\mathrm{i}k_*\eta_{\gamma,c}]/\lambda_-.\end{aligned} \tag{A.8}$$

It can be checked that, indeed, $(x_{1j},y_{1j})^{\mathrm{T}}\in\operatorname{Rg}\mathcal{M}_{\mathrm{i}\omega_*}(a_*,k_*,c)$. At order $\mathcal{O}(\varepsilon E^2)$ we find

$$\begin{pmatrix}X_{22}\\Y_{22}\end{pmatrix}=\begin{pmatrix}x_{22}\\y_{22}\end{pmatrix}\mathcal{A}^2,$$

with

$$\begin{aligned}x_{22}&=\left(\frac{b}{a_*}\right)^2\left(4k_*^2+2\mathrm{i}\omega_*-b\right)y_{22}-\left(\frac{b}{a_*}\right)^2\left(\frac{b^2}{a_*}\eta_{\gamma,c}^2+4a_*\eta_{\gamma,c}\right),\\ y_{22}&=\frac{\frac{b^2}{a_*}\eta_{\gamma,c}^2+4a_*\eta_{\gamma,c}+8b^2k_*^2\gamma(\gamma-1)(\frac{b^2}{a_*})^{\gamma-2}}{(\frac{b^2}{a_*})^2(4k_*^2+2\mathrm{i}\omega_*-b)(-4\Gamma k_*^2-(\frac{a_*}{b})^2+2\mathrm{i}ck_*)-2b}\\ &\quad+\frac{(\frac{b}{a_*})^2(\frac{b^2}{a_*}\eta_{\gamma,c}^2+4a_*\eta_{\gamma,c})(-4\Gamma k_*^2-(\frac{a_*}{b})^2+2\mathrm{i}ck_*)}{(\frac{b^2}{a_*})^2(4k_*^2+2\mathrm{i}\omega_*-b)(-4\Gamma k_*^2-(\frac{a_*}{b})^2+2\mathrm{i}ck_*)-2b}.\end{aligned} \tag{A.9}$$

At order $\varepsilon^2 E$, we obtain equations for X_{13} and Y_{13}. These equations can be written as

$$\mathcal{M}_{\omega_*}(a_*, k_*, c)\begin{pmatrix} X_{13} \\ Y_{13} \end{pmatrix} = \begin{pmatrix} I_1 \\ I_2 \end{pmatrix}. \tag{A.10}$$

The right-hand sides I_1, I_2 are built up by several terms. The nonlinear terms from the reaction kinetics generate

$$\begin{aligned} 2\frac{a_*}{b}UV &\to 2\frac{a_*}{b}[2by_{22} + \eta_{\gamma,c}x_{02} + \bar{\eta}_{\gamma,c}x_{22}], \\ \frac{b^2}{a_*}V^2 &\to \frac{b^2}{a_*}[2\bar{\eta}_{\gamma,c}y_{22}], \\ UV^2 &\to 4b|\eta_{\gamma,c}|^2 + 2b\eta_{\gamma,c}^2. \end{aligned}$$

We define L_{tot} as the sum of these expressions:

$$L_{\mathrm{tot}} := \left(2\bar{\eta}_{\gamma,c}\frac{b^2}{a_*} + 4a_*\right)y_{22} + 2\frac{a_*}{b}(\eta_{\gamma,c}x_{02} + \bar{\eta}_{\gamma,c}x_{22}) + 2b\big(2|\eta_{\gamma,c}|^2 + \eta_{\gamma,c}^2\big). \tag{A.11}$$

The nonlinear terms that appear from working out the nonlinear diffusion terms generate

$$\begin{aligned} U_{xx}U &\to -2bk_*^2(x_{02} + 5x_{22})\gamma(\gamma-1)\left(\frac{b^2}{a_*}\right)^{\gamma-2}, \\ (U_x)^2 &\to 8bk_*^2x_{22}\gamma(\gamma-1)\left(\frac{b^2}{a_*}\right)^{\gamma-2}, \\ \frac{1}{2}U_{xx}U^2 &\to -12b^3k_*^2\gamma(\gamma-1)(\gamma-2)\left(\frac{b^2}{a_*}\right)^{\gamma-3}, \\ (U_x)^2U &\to 8b^3k_*^2\gamma(\gamma-1)(\gamma-2)\left(\frac{b^2}{a_*}\right)^{\gamma-3}, \\ U_{xx} &\to -2bk_*^2. \end{aligned}$$

Based on this we define

$$\begin{aligned} L_{\mathrm{NLD}} &= -2bk_*^2(x_{22} + x_{02})\gamma(\gamma-1)\left(\frac{b^2}{a_*}\right)^{\gamma-2} \\ &\quad - 4b^3k_*^2\gamma(\gamma-1)(\gamma-2)\left(\frac{b^2}{a_*}\right)^{\gamma-3}, \\ L_{\mathcal{A},\mathrm{NLD}} &= -k_*^2\gamma(\gamma-1)\frac{2b}{a_*}\left(\frac{b^2}{a_*}\right)^{\gamma-2}. \end{aligned}$$

We then obtain for the right-hand side of the system

$$\begin{aligned} I_1 &= \left(-4\frac{a_*}{b} - L_{\mathcal{A},\mathrm{NLD}}\right)\mathcal{A} + (L_{\mathrm{tot}} - L_{\mathrm{NLD}})|\mathcal{A}|^2\mathcal{A} \\ &\quad - (cx_{12} + 2b\Gamma + 2\mathrm{i}k_*\Gamma x_{12})\mathcal{A}_{\xi\xi}, \\ I_2 &= 4\frac{a_*}{b}\mathcal{A} - L_{\mathrm{tot}}|\mathcal{A}|^2\mathcal{A} - (c_{\mathrm{g}}y_{12} + \eta_{\gamma,c} + 2\mathrm{i}k_*y_{12})\mathcal{A}_{\xi\xi} + \eta_{\gamma,c}\mathcal{A}_\tau. \end{aligned} \tag{A.12}$$

To derive the Ginzburg–Landau equation, we impose the solvability condition (2.42) to (A.10):

$$2bI_2 - \big(k_*^2 + \mathrm{i}\omega_* - b\big)I_1 = 0, \tag{A.13}$$

and obtain

$$\begin{aligned} 2b\eta_{\gamma,c}\mathcal{A}_\tau = {} & \big[2b(\mathrm{c_g}y_{12} + \eta_{\gamma,c} + 2\mathrm{i}k_* y_{12}) \\ & - \big(k_*^2 + \mathrm{i}\omega_* - b\big)(cx_{12} + 2b\Gamma + 2\mathrm{i}k_*\Gamma x_{12})\big]\mathcal{A}_{\xi\xi} \\ & - \left[4\frac{a_*}{b}\big(k_*^2 + \mathrm{i}\omega_* + b\big) + \big(k_*^2 + \mathrm{i}\omega_* - b\big)L_{\mathcal{A},\mathrm{NLD}}\right]\mathcal{A} \\ & + \big[\big(k_*^2 + \mathrm{i}\omega_* + b\big)L_{\mathrm{tot}} - \big(k_*^2 + \mathrm{i}\omega_* - b\big)L_{\mathrm{NLD}}\big]|\mathcal{A}|^2\mathcal{A}. \end{aligned}$$

A.1 The Special Case that $\gamma = 1$ and $c = \sqrt{\frac{2}{3}b}$

In this section we present the expressions for x_{ij}, y_{ij}, $ij = 02, 12, 22$ for the special case that $\gamma = 1$ and $c = \sqrt{\frac{2}{3}b}$. In Proposition 2 we computed that for $\gamma = 1$ and $c = \sqrt{\frac{2}{3}b}$ one has

$$k_*^2 = \frac{1}{3}b, \qquad a_*^2 = \frac{1}{3}b^3, \qquad \omega_* = -\frac{1}{3}b\sqrt{2} \quad \text{and} \quad c_\mathrm{g} = -\sqrt{\frac{2}{3}b}.$$

Also, one computes the second component of a basis vector of the kernel of $\mathcal{M}_{\omega_*}(a_*, k_*, c)$ and the nonzero eigenvalue of $\mathcal{M}_{\omega_*}(a_*, k_*, c)$ as

$$\eta_{1,\sqrt{\frac{2}{3}b}} = \frac{1}{3}b(-2 + \mathrm{i}\sqrt{2}) \quad \text{and} \quad \lambda_+ = \frac{2}{3}b\mathrm{i}\sqrt{2}.$$

These values are used to derive

$$\begin{aligned} x_{02} &= 4b\sqrt{\frac{b}{3}}, \\ y_{02} &= 0, \\ x_{12} &= -\frac{1}{2}\sqrt{6b}\,(2 - \mathrm{i}\sqrt{2}), \\ y_{12} &= \frac{1}{2}\sqrt{6b}, \\ x_{22} &= \frac{2}{33}b\sqrt{\frac{b}{3}}(23 + 26\mathrm{i}\sqrt{2}), \\ y_{22} &= -\frac{2}{33}b\sqrt{\frac{b}{3}}(20 + 14\mathrm{i}\sqrt{2}). \end{aligned}$$

The nonlinear terms from the reaction kinetics are

$$2\frac{a_*}{b}UV \to -\frac{4}{99}b^3(82+31\mathrm{i}\sqrt{2}),$$
$$\frac{b^2}{a_*}V^2 \to \frac{48}{99}b^3(1+4\mathrm{i}\sqrt{2}),$$
$$UV^2 \to \frac{4}{9}b^3(7-2\mathrm{i}\sqrt{2}).$$

The sum of these expressions is

$$L_{\mathrm{tot}} := \frac{4}{99}(7-5\mathrm{i}\sqrt{2}).$$

The nonlinear diffusion terms are, of course, zero, so $L_{\mathrm{NLD}} = L_{\mathcal{A},\mathrm{NLD}} = 0$. We get for the right hand components as in (A.10):

$$\frac{b}{3}I_1 = -4\sqrt{\frac{3}{b}}A + \frac{4}{33}b^2(7-5\mathrm{i}\sqrt{2})|\mathcal{A}|^2\mathcal{A} + (6+3\mathrm{i}\sqrt{2})\mathcal{A}_{\xi\xi},$$
$$\frac{b}{3}I_2 = 4\sqrt{\frac{3}{b}}A - \frac{4}{33}b^2(7-5\mathrm{i}\sqrt{2})|\mathcal{A}|^2\mathcal{A} + (5-4\mathrm{i}\sqrt{2})\mathcal{A}_{\xi\xi} - (2-\mathrm{i}\sqrt{2})\mathcal{A}_{\tau}.$$

These give the Ginzburg–Landau equation in (2.51):

$$\mathcal{A}_\tau = \frac{1}{3}(8+\mathrm{i}\sqrt{2})\mathcal{A}_{\xi\xi} + \frac{2}{9}\sqrt{\frac{3}{b}}(5+\mathrm{i}\sqrt{2})\mathcal{A} - \frac{2}{33}(5-2\mathrm{i}\sqrt{2})b^2|\mathcal{A}|^2\mathcal{A}.$$

A.2 Derivation of the Ginzburg–Landau Equation for the GKGS-System with $c = 0$

In this section we present the expressions for x_{ij}, y_{ij}, $ij = 02, 12, 22$ for the special case that $c = 0$. In Proposition 1 we computed that for $c = 0$ one has

$$k_*^2 = \frac{1}{2}(1-g)b, \quad \text{and} \quad a_*^{\gamma+1} = g\gamma b^{2\gamma+1}.$$

Also, one computes the second component of a basis vector of the kernel of $\mathcal{M}_{\omega_*}(a_c, k_c, c)$ and the nonzero eigenvalue of $\mathcal{M}_{\omega_*}(a_c, k_c, c)$ as

$$\eta_{\gamma,0} = \frac{1}{2}(g-7)\frac{a_*^2}{b^2} \quad \text{and} \quad \lambda_- = \frac{1}{2}(g-7)\frac{a_*^2}{b^2} + \frac{1}{2}(1+g)b.$$

These values are used to derive

$$x_{02} = 4a_*,$$
$$y_{02} = 0,$$
$$x_{12} = 0,$$
$$y_{12} = 2\mathrm{i}(6-g)\frac{a_*^2}{b^3}k_*,$$

$$x_{22} = \frac{2}{9}\big[9 - 2(3+g)\gamma\big]a_*,$$
$$y_{22} = -\frac{4}{9}(5-g)\gamma\frac{a_*^3}{b^3}.$$

The sum of the nonlinear terms from the kinetics is

$$L_{\text{tot}} := \left[\frac{8}{9}(18-2g)\gamma + 6(5-g)\right]\frac{a_*^4}{b^3}.$$

Also we have

$$L_{\text{NLD}} = -2bk_*^2(x_{02}+x_{22})\gamma(\gamma-1)\left(\frac{b^2}{a_*}\right)^{\gamma-2} - 4b^3k_*^2\gamma(\gamma-1)(\gamma-2)\left(\frac{b^2}{a_*}\right)^{\gamma-3},$$
$$L_{\text{NLD},\mathcal{A}} = -(1-5g)(\gamma-1)\frac{a_*}{b}.$$

This gives the Ginzburg–Landau equation in (2.49):

$$\mathcal{A}_\tau = 2\sqrt{2}\,\mathcal{A}_{\xi\xi} + b_1(\gamma)\mathcal{A} + \mathcal{L}_1(\gamma)|\mathcal{A}|^2\mathcal{A}$$

with

$$b_1(\gamma) = \big[-39 + 27\sqrt{2} + (41 - 29\sqrt{2})\gamma\big]\left(\frac{g\gamma}{b}\right)^{\frac{1}{\gamma+1}},$$
$$\mathcal{L}_1(\gamma) = -\frac{1}{9}(2-\sqrt{2})\big[18(3+2\sqrt{2}) + 12(2+\sqrt{2})\gamma + (-8+3\sqrt{2})\gamma^2\big] \times \left(\frac{g\gamma}{b}\right)^{\frac{2}{\gamma+1}} b^3.$$

A.3 Derivation of the Ginzburg–Landau Equation for the Case $c \gg 1$: The Klausmeier Model and the GKGS-Model for $c \gg 1$

This appendix to Sect. 2.6 deals with an elaborate account on the scalings introduced in Sect. 2.6 that were used to derive the Klausmeier system (2.53) from the GKGS-system. Also, we derive the GLE for the Klausmeier system (2.53).

Scaling Analysis for the Klausmeier System as a Limit Case of the GKGS System We remark that the equilibria for both systems (1.5) and (2.53) are the same. Patterns close to the equilibrium (U_+, V_+) can be described as

$$\begin{aligned} U &= \delta^{2\beta-\alpha}\big(\hat{U}_+ + \varepsilon\hat{U}(x,t)\big);\\ V &= \delta^{\alpha-\beta}\big(\hat{V}_+ + \varepsilon\hat{V}(x,t)\big). \end{aligned} \tag{A.14}$$

Substitution of these expansions in (1.5) gives the leading order formulation (2.38). We are interested in the behavior of the GKGS-model for $0 < 1/\sqrt{c} \ll \varepsilon \ll 1$. Since

we know from Proposition 2 that $a_c = \mathcal{O}(\sqrt{c})$, we put $a_* = \bar{a}_*\sqrt{c}$ and obtain for (2.38),

$$\begin{aligned}
\delta^{3\beta-2\alpha}U_t &= c^{-\frac{1}{2}(\gamma-1)}\gamma\left(\frac{b^2}{\bar{a}_*}\right)^{\gamma-1}U_{xx} + cU_x - \left[c\frac{\bar{a}_*^2}{b^2}U + 2bV\right] \\
&\quad + \varepsilon\left[\gamma(\gamma-1)\left(\frac{b^2}{\bar{a}_*\sqrt{c}}\right)^{\gamma-2}\left[U_{xx}U + (U_x)^2\right]\right. \\
&\quad \left. - \frac{b^2}{\bar{a}_*\sqrt{c}}V^2 - 2\frac{\bar{a}_*}{b}\sqrt{c}UV\right] \\
&\quad + \varepsilon^2\left[\gamma(\gamma-1)(\gamma-2)\left(\frac{b^2}{\bar{a}_*\sqrt{c}}\right)^{\gamma-3}\left[U(U_x)^2 + \frac{1}{2}U^2U_{xx}\right]\right. \\
&\quad \left. + \gamma(\gamma-1)\frac{1}{\bar{a}_*\sqrt{c}}\left(\frac{b^2}{\bar{a}_*\sqrt{c}}\right)^{\gamma-1}U_{xx} + 2r\frac{\bar{a}_*}{b^2}\sqrt{c}U - UV^2\right], \\
V_t &= V_{xx} + \left[\frac{\bar{a}_*^2c}{b^2}U + bV\right] + \varepsilon\left[\frac{b^2}{\bar{a}_*\sqrt{c}}V^2 + 2\frac{\bar{a}_*}{b}\sqrt{c}UV\right] \\
&\quad - \varepsilon^2\left[2r\frac{\bar{a}_*}{b^2}\sqrt{c}U - UV^2\right].
\end{aligned} \tag{A.15}$$

In order to derive the Klausmeier model, we must scale the components U and V such that the diffusion coefficient in the first component of (2.38) is of higher order in $1/\sqrt{c}$ than the other terms in the equations. The other terms must balance at the same, highest order. In order to obtain this, we scale U, V, and r such that

$$U = \frac{\bar{U}}{\sqrt{c}}, \qquad V = \sqrt{c}\bar{V} \quad \text{and} \quad r = \bar{r}\sqrt{c}. \tag{A.16}$$

With these scalings we obtain for (A.15), by neglecting higher orders of δ and $1/\sqrt{c}$,

$$\begin{aligned}
0 &= \bar{U}_{\tilde{x}} - \left[\frac{\bar{a}_*^2}{b^2}\bar{U} + 2b\bar{V}\right] - \varepsilon\left[\frac{b^2}{\bar{a}_*}\bar{V}^2 + 2\frac{\bar{a}_*}{b}\bar{U}\bar{V}\right] + \varepsilon^2\left[2\bar{r}\frac{\bar{a}_*}{b^2}\bar{U} - \bar{U}\bar{V}^2\right], \\
\bar{V}_{\tilde{t}} &= \bar{V}_{\tilde{x}\tilde{x}} + \left[\frac{\bar{a}_*^2}{b^2}\bar{U} + b\bar{V}\right] + \varepsilon\left[\frac{b^2}{\bar{a}_*}\bar{V}^2 + 2\frac{\bar{a}_*}{b}\bar{U}\bar{V}\right] - \varepsilon^2\left[2\bar{r}\frac{\bar{a}_*}{b^2}\bar{U} - \bar{U}\bar{V}^2\right].
\end{aligned} \tag{A.17}$$

We can now scale out b by putting

$$\begin{aligned}
&\bar{U} = \tilde{U}b^{3/4}; \qquad \bar{V} = \tilde{b}^{1/4}V; \qquad \bar{a}_c = \tilde{a}_cb^{5/4}; \\
&x = b^{-1/2}\tilde{x}; \qquad t = b^{-1/4}\tilde{t}; \qquad \bar{r} = \tilde{r}b^{5/4},
\end{aligned} \tag{A.18}$$

and obtain, to leading order in ε and neglecting higher order terms of δ and $\frac{1}{\sqrt{c}}$,

$$\begin{aligned} 0 &= \tilde{U}_{\tilde{x}} - \big[\tilde{a}_*^2\tilde{U} + 2\tilde{V}\big] - \varepsilon\left[\frac{1}{\tilde{a}_*}\tilde{V}^2 + 2\tilde{a}_*\tilde{U}\tilde{V}\right] + \varepsilon^2\big[2\tilde{r}\tilde{a}_*\tilde{U} - \tilde{U}\tilde{V}^2\big], \\ \tilde{V}_{\tilde{t}} &= \tilde{V}_{\tilde{x}\tilde{x}} + \big[\tilde{a}_*^2\tilde{U} + \tilde{V}\big] + \varepsilon\left[\frac{1}{\tilde{a}_*}\tilde{V}^2 + 2\tilde{a}_*\tilde{U}\tilde{V}\right] - \varepsilon^2\big[2\tilde{r}\tilde{a}_*\tilde{U} - \tilde{U}\tilde{V}^2\big]. \end{aligned} \tag{A.19}$$

This system is the one presented in (2.55).

Derivation of the GLE for the Klausmeier System: The Regime $0 < 1/\sqrt{c} \ll \varepsilon \ll 1$ From (A.19) one derives the dispersion relation associated to the linearization about the background state (U_+, V_+) in the Klausmeier model, neglecting higher orders of ε,

$$\det \mathcal{M}_\lambda(\tilde{a}_*, \mathrm{i}\tilde{k}) := \det\begin{pmatrix} -\tilde{a}_*^2 + \mathrm{i}\tilde{k} & -2 \\ \tilde{a}_*^2 & 1 - \tilde{k}^2 - \tilde{\lambda} \end{pmatrix} = 0. \tag{A.20}$$

We apply conditions (2.7a), (2.7b) to derive critical parameters. Working out the dispersion relation (A.20) using condition (2.7a),

$$\mathrm{i}\tilde{\omega}\tilde{a}_*^2 + \mathrm{i}\tilde{k}\big(1 - \tilde{k}^2\big) = 0; \tag{A.21a}$$

$$\tilde{\omega}\tilde{k} + \big(\tilde{k}^2 - 1\big)\tilde{a}_*^2 + 2\tilde{a}_*^2 = 0. \tag{A.21b}$$

From these relations one derives

$$\tilde{k}^2\big(\tilde{k}^2 - 1\big) + \tilde{a}_*^4\big(\tilde{k}^2 + 1\big) = 0, \tag{A.22}$$

and by solving equation (A.21a) for $\tilde{\omega}$ we get

$$\tilde{\omega}_* = \tilde{k}_*\big(\tilde{k}_*^2 - 1\big)\frac{1}{\tilde{a}_*^2}, \tag{A.23}$$

and thus

$$\frac{\partial\tilde{\omega}}{\partial\tilde{k}} = \frac{1}{\tilde{a}_*^2}\big(3\tilde{k}^2 - 1\big). \tag{A.24}$$

Differentiating (A.24) with respect to $\tilde{k}$ and substituting equation (A.21b) into the result, we get

$$2\tilde{k}^2 - 1 + \tilde{a}_*^4 = 0. \tag{A.25}$$

Solving (A.22) and (A.25) for $\tilde{a}$ and $\tilde{k}$ then gives

$$\tilde{a}_*^2 = \sqrt{2} - 1 \quad \text{and} \quad \tilde{k}_*^2 = \sqrt{2} - 1, \tag{A.26}$$

which are the expressions for large c that we had derived in Proposition 2. From these expressions for $\tilde{a}_*$ and $\tilde{k}_*$ we further derive the critical frequency and the group speed

$$\begin{aligned} \tilde{\omega}_* &= -\sqrt{2}\sqrt{\sqrt{2}-1}; \\ \tilde{c}_{\mathrm{g}} &= -\frac{\partial\tilde{\omega}}{\partial\tilde{k}}\bigg|_{k=k_*} = -2+\sqrt{2}. \end{aligned} \tag{A.27}$$

From (A.20) it follows that the kernel and range of the linearization about the equilibrium $(\tilde{U}_+, \tilde{V}_+)$ equal

$$\ker \mathcal{M}_{\mathrm{i}\tilde{\omega}_*}(\tilde{a}_*, \tilde{k}_*) = \begin{pmatrix} 2 \\ -\tilde{a}_*^2 + \mathrm{i}k_* \end{pmatrix} \tag{A.28}$$

and

$$\mathrm{Rg}\, \mathcal{M}_{\mathrm{i}\tilde{\omega}_*}(\tilde{a}_*, \tilde{k}_*) = \begin{pmatrix} -2 \\ 1-\tilde{k}_*^2 - \mathrm{i}\tilde{\omega}_* \end{pmatrix}.$$

From the expression for the range of $\mathcal{M}_{\mathrm{i}\tilde{\omega}_*}(\tilde{a}_*, \tilde{k}_*)$ we derive that the equations

$$\mathcal{M}_{\mathrm{i}\tilde{\omega}}(\tilde{a}_*, \tilde{k}_*)x = f$$

can be solved for x if and only if $f \in \mathrm{Rg}\, \mathcal{M}_{\mathrm{i}\tilde{\omega}_*}(\tilde{a}_*, \tilde{k}_*)$, that is, if f fulfills the *solvability condition*

$$2f_2 + \left[1 - \tilde{k}_*^2 - \mathrm{i}\tilde{\omega}_*\right] f_1 = 0. \tag{A.29}$$

Since $\mathrm{Det}\, \mathcal{M}_{\mathrm{i}\tilde{\omega}_*}(\tilde{a}_*, \tilde{k}_*) = 0$, it follows that the unique solution to the equation $\mathcal{M}_{\mathrm{i}\tilde{\omega}_*}(\tilde{a}_*, \tilde{k}_*)x = f$ is

$$x = \frac{1}{\lambda_-} f$$

with λ_- the nonzero eigenvalue of $\mathcal{M}_{\mathrm{i}\tilde{\omega}_*}(\tilde{a}_*, \tilde{k}_*)$,

$$\lambda_- := \mathrm{Tr}\, \mathcal{M}_{\mathrm{i}\tilde{\omega}}(\tilde{a}_*, \tilde{k}_*) = -\tilde{a}_*^2 + \mathrm{i}k_* + 1 - \tilde{k}_*^2 - \mathrm{i}\tilde{\omega}_*. \tag{A.30}$$

By using (A.28), the expansion (U, V) that describes the pattern near its onset (i.e., for $\tilde{a} = \tilde{a}_* - \tilde{r}\varepsilon^2$) can be written out as

$$\begin{pmatrix} U \\ V \end{pmatrix} = \mathcal{A}(\xi, \tau) \begin{pmatrix} 2 \\ \eta \end{pmatrix} \mathrm{e}^{\mathrm{i}(\tilde{k}_* x + \tilde{\omega}_* t)} + \mathrm{c.c.} + \mathrm{h.o.t.}, \tag{A.31}$$

with the shorthand

$$\eta := -\tilde{a}_*^2 + \mathrm{i}\tilde{k}_*.$$

As pointed out in at the begin of the Appendix, in the Ginzburg–Landau formalism one subsequently derives equations of the form $X_{02} = x_{02}\mathcal{A}^2$, $Y_{02} = y_{02}\mathcal{A}^2$, $X_{12} = x_{12}\mathcal{A}_\xi$, $Y_{12} = y_{12}\mathcal{A}_\xi$, $X_{22} = x_{22}|\mathcal{A}|^2$, and $Y_{22} = y_{22}|\mathcal{A}|^2$. The formulas for x_{ij} and y_{ij}

are derived by substituting the expansion (A.31) in the leading order system (A.19) and collecting terms of order $\varepsilon^{j-1}E^i$ (with shorthand $E = \mathrm{e}^{\mathrm{i}(\tilde{k}_c x+\tilde{\omega}_c t)}$) and solving them for X_{ij} and Y_{ij}:

$$\begin{aligned}
x_{02} &= -2\frac{1}{\tilde{a}_*^3}|\eta|^2 - 4\frac{1}{\tilde{a}_*}(\bar{\eta}+\eta),\\
y_{02} &= 0,\\
x_{12} &= \frac{-2}{\lambda_-},\\
y_{12} &= \frac{1}{\lambda_-}(\eta c_{\mathrm{g}} - 2\eta \mathrm{i}\tilde{k}_c),\\
x_{22} &= \frac{2\mathrm{i}\tilde{k}_*[\frac{1}{\tilde{a}_*}\eta^2 + 4\tilde{a}_*\eta]}{[-\tilde{a}_*^2 + 2\mathrm{i}\tilde{k}_*]\cdot[4\tilde{k}_*^2 + 2\mathrm{i}\tilde{\omega}_* - 1] - 2\tilde{a}_*^2},\\
y_{22} &= \frac{1}{\tilde{a}_*^2}\big[4\tilde{k}_*^2 + 2\mathrm{i}\tilde{\omega} - 1\big]x_{22} - \frac{1}{\tilde{a}_*^2}\bigg[\frac{1}{\tilde{a}_*}\eta^2 + 4\tilde{a}_*\eta\bigg].
\end{aligned} \tag{A.32}$$

The Ginzburg–Landau equation that describes the onset of patterns in the Klausmeier system (A.19) reads

$$\begin{aligned}
2\eta A_\tau = &-\big[2(c_g y_{12} - \eta - 2\mathrm{i}\tilde{k}_* y_{12}) - x_{12}\big(1 - \tilde{k}_*^2 - \mathrm{i}\tilde{\omega}_*\big)\big]A_{\xi\xi}\\
&- 4\tilde{r}\tilde{a}_*\,[1 + \tilde{k}_* + \mathrm{i}\tilde{\omega}]\,A + [1 + \tilde{k}_* + \mathrm{i}\tilde{\omega}]\,L_{\mathrm{tot}}\,|A|^2 A
\end{aligned} \tag{A.33}$$

with

$$L_{\mathrm{tot}} = \frac{2\bar{\eta}}{\tilde{a}_*}y_{22} + 4\tilde{a}_*^2 y_{22} + 2\tilde{a}_*\eta x_{02} + 2\tilde{a}_*\bar{\eta}x_{22} + 4|\eta|^2 + 2\eta^2.$$

If one works out the parameter values for $\tilde{a}_*^2 = \sqrt{2}-1$ and $\tilde{k}_*^2 = \sqrt{2}-1$, the leading order system (A.19) becomes

$$\begin{aligned}
0 = {} & \tilde{U}_{\tilde{x}} - \big[(\sqrt{2}-1)\tilde{U} + 2\tilde{V}\big]\\
& - \varepsilon\bigg[\frac{1}{\sqrt{\sqrt{2}-1}}\tilde{V}^2 + 2\sqrt{\sqrt{2}-1}\tilde{U}\tilde{V}\bigg] + \varepsilon^2\Big[2\tilde{r}\sqrt{\sqrt{2}-1}\tilde{U} - \tilde{U}\tilde{V}^2\Big],\\
\tilde{V}_{\tilde{t}} = {} & \tilde{V}_{\tilde{x}\tilde{x}} + \big[(\sqrt{2}-1)\tilde{U} + \tilde{V}\big]\\
& + \varepsilon\bigg[\frac{1}{\sqrt{\sqrt{2}-1}}\tilde{V}^2 + 2\sqrt{\sqrt{2}-1}\tilde{U}\tilde{V}\bigg] - \varepsilon^2\Big[2\tilde{r}\sqrt{\sqrt{2}-1}\tilde{U} - \tilde{U}\tilde{V}^2\Big].
\end{aligned} \tag{A.34}$$

The matrix that describes the linear leading order part of this system is then

$$\mathcal{M}_\lambda(\tilde{a}_*, k) := \begin{pmatrix} -\sqrt{2}+1+\mathrm{i}\sqrt{\sqrt{2}-1} & -2\\ \sqrt{2}-1 & 2-\sqrt{2}+\mathrm{i}\sqrt{2}\sqrt{\sqrt{2}-1}\end{pmatrix}. \tag{A.35}$$

Working out the levels for the different expressions (A.32), we get

$$\begin{aligned}
x_{02} &= (4-2\sqrt{2})\sqrt{\sqrt{2}-1},\\
y_{02} &= 0,\\
x_{12} &= -\frac{1}{41}\Big[10-3\sqrt{2}-\mathrm{i}(40+29\sqrt{2})\sqrt{\sqrt{2}-1}\Big],\\
y_{12} &= \frac{1}{82}\Big[78\sqrt{2}-96+\mathrm{i}(16\sqrt{2}-108)\sqrt{\sqrt{2}-1}\Big],\\
x_{22} &= \frac{1}{69}\Big[(61\sqrt{2}+40)\sqrt{\sqrt{2}-1}+2\mathrm{i}(67\sqrt{2}-13)\Big],\\
y_{22} &= -\frac{2}{69}\Big[(10\sqrt{2}+42)\sqrt{\sqrt{2}-1}+\mathrm{i}(5\sqrt{2}-2)\Big],
\end{aligned} \tag{A.36}$$

and

$$L_{\mathrm{tot}} = -44+32\sqrt{2}+\mathrm{i}[-20+18\sqrt{2}]\sqrt{\sqrt{2}-1}.$$

The Ginzburg–Landau equation then becomes

$$\begin{aligned}
&-2\Big[\sqrt{2}-1+\mathrm{i}\sqrt{\sqrt{2}-1}\Big]\mathcal{A}_\tau\\
&\quad= -\frac{1}{41}\Big[594-416\sqrt{2}+\mathrm{i}(330-304\sqrt{2})\sqrt{\sqrt{2}-1}\Big]\mathcal{A}_{\xi\xi}\\
&\qquad-4\tilde{r}\Big[\sqrt{2}\sqrt{\sqrt{2}-1}-\mathrm{i}(2-\sqrt{2})\Big]\mathcal{A}\\
&\qquad+\frac{4}{69}\Big[-885+637\sqrt{2}+\mathrm{i}(183-170\sqrt{2})\sqrt{\sqrt{2}-1}\Big]|\mathcal{A}|^2\mathcal{A}
\end{aligned}$$

or, equivalently,

$$\begin{aligned}
\mathcal{A}_\tau &= \frac{1}{41}\Big[(66-56\sqrt{2})-\mathrm{i}(63-23\sqrt{2})\sqrt{\sqrt{2}-1}\Big]\mathcal{A}_{\xi\xi}\\
&\quad+\tilde{r}\Big[4\sqrt{\sqrt{2}-1}+\mathrm{i}(4-2\sqrt{2})\Big]\mathcal{A}\\
&\quad+\frac{4}{69}\Big[-807+534\sqrt{2}+\mathrm{i}(418-286\sqrt{2})\sqrt{\sqrt{2}-1}\Big]|\mathcal{A}|^2\mathcal{A}
\end{aligned}$$

which is the equation presented in (2.56).

The GLE for the GKGS Model for $c \gg 1$: The Regime $0 < \varepsilon \ll 1/\sqrt{c} \ll 1$ As in the previous section, we scale the leading order system of the GKGS model according to (2.54). We then obtain the leading order system (2.57). To first order in ε, the leading

order system (2.57) reads

$$\mathcal{M}^c_\lambda(\tilde a_*, \mathrm{i}\tilde k) := \begin{pmatrix} -\gamma a_*^{1-\gamma} c^{-\frac{1}{2}\gamma} b^{\frac{3}{4}\gamma-\frac{1}{4}} \tilde k^2 + c^{\frac{1}{2}}[\mathrm{i}\tilde k - \tilde a_*^2] & -2c^{\frac{1}{2}} \\ \tilde a_*^2 & 1-\tilde k^2-\tilde\lambda \end{pmatrix}. \tag{A.37}$$

First, we remark that for $\gamma \geq 1$ the linear part of the nonlinear diffusion in the GKGS-model is in leading order $\leq \mathcal{O}(c^{-1/2})$. Secondly, we remark that to leading order in c,

$$\det \mathcal{M}^c_\lambda(\tilde a_*, \mathrm{i}\tilde k) = c^{\frac{1}{2}} \mathcal{M}_\lambda(\tilde a_*, \mathrm{i}\tilde k) + \mathcal{O}\big(c^{\frac{1}{2}(1-\gamma)}\big)$$

with $\mathcal{M}_\lambda(\tilde a_*, \mathrm{i}\tilde k)$ as defined in (A.20). Therefore, the critical $\tilde k_*$, $\tilde a_*$, $\tilde\omega_*$, and $\tilde c_g$ are to leading order in c as in (A.26) and (A.27).

The solvability condition is as in (A.29). Using the leading order system (2.57), we compute

$$\begin{aligned}
x_{02} &= -2\frac{1}{\tilde a_*^3}|\eta|^2 - 4\frac{1}{\tilde a_*}(\bar\eta + \eta), \\
y_{02} &= 0, \\
x_{12} &= \frac{l_0 \cdot c^{-\frac{1}{2}\gamma} - 2}{\lambda_-}, \\
y_{12} &= \frac{1}{\lambda_-}(\eta c_{\mathrm{g}} - 2\eta \mathrm{i}\tilde k_c), \\
x_{22} &= \frac{1}{\tilde a_*^2}\big[4\tilde k_*^2 + 2\mathrm{i}\tilde\omega - 1\big] y_{22} - \frac{1}{\tilde a_*^2}\left[\frac{1}{\tilde a_*}\eta^2 + 4\tilde a_*\eta\right], \\
y_{22} &= \frac{-l_1 c^{-\theta_1} - l_2 c^{-\theta_2}\frac{1}{\tilde a_*}\eta^2 + 4\tilde a_*\eta + \frac{1}{a^2}[-l_3 c^{-\theta_2} - a^2 + 2\mathrm{i}\tilde k][\frac{1}{a}\eta^2 + 4a\eta]}{[l_4 c^{-\theta_4} - \tilde a_*^2 + 2\mathrm{i}\tilde k_*]\cdot[4\tilde k_*^2 + 2\mathrm{i}\tilde\omega_* - 1] - 2\tilde a_*^2}.
\end{aligned} \tag{A.38}$$

In (A.38) it is understood that all l_i, $i = 0, \ldots, 4$ do not depend on c and that $\theta_i \geq 0$ for $i = 0, \ldots, 4$. We have not computed the l_i and θ_i explicitly. This gives for the GLE of the GKGS-model in general form

$$\begin{aligned}
2\eta \mathcal{A}_\tau = &-\big[2(c_g y_{12} - \eta - 2\mathrm{i}\tilde k_* y_{12}) - \big(x_{12} + \mathrm{const}\cdot c^{-\frac{1}{2}\gamma}\big)\big(1 - \tilde k_*^2 - \mathrm{i}\tilde\omega_*\big)\big]\mathcal{A}_{\xi\xi} \\
&- \big[4\tilde r \tilde a_*\big(1 + \tilde k_*^2 + \mathrm{i}\tilde\omega\big) + \big(\tilde k_*^2 + \mathrm{i}\tilde\omega - 1\big) L_{\mathcal{A},\mathrm{NLD}}\big]\mathcal{A} \\
&+ \big[\big(1 + \tilde k_*^2 + \mathrm{i}\tilde\omega\big) L_{\mathrm{tot}} - \big(\tilde k_*^2 + \mathrm{i}\tilde\omega - 1\big) L_{\mathrm{NLD}}\big]|\mathcal{A}|^2\mathcal{A}
\end{aligned} \tag{A.39}$$

with

$$\begin{aligned}
L_{\mathrm{NLD}} &= -\tilde k_*^2 (x_{22} + x_{02}) \cdot \mathrm{const} \cdot c^{-\frac{1}{2}(1+\gamma)} - 4\tilde k_*^2 \cdot \mathrm{const} \cdot c^{-\frac{1}{2}(1+\gamma)}, \\
L_{\mathcal{A},\mathrm{NLD}} &= -\tilde k_* \cdot \mathrm{const} \cdot c^{-\frac{1}{2}\gamma}.
\end{aligned}$$

We have not bothered about calculating the constant denoted by "const", since for asymptotically large c the associated expressions only play a role at higher order.

That is, for asymptotically large $c \gg 1$ it is immediate that (A.39) reduces to (A.33). Using the expressions (A.38) and inserting $\tilde{k}$, $\tilde{a}$, $\tilde{\omega}$, and c_g one obtains the GLE for the Klausmeier system (2.56).

References

Amann, H.: Dynamic theory of quasilinear parabolic equations II. Reaction–diffusion systems. Differ. Integral Equ. **3**, 13–75 (1990)

Aranson, I., Kramer, L.: The world of the complex Ginzburg–Landau equation. Rev. Mod. Phys. **74**, 187–214 (2002)

Busse, F.H.: Nonlinear properties of thermal convection. Rep. Prog. Phys. **41**, 1929–1967 (1978)

Chen, W., Ward, M.J.: Oscillatory instabilities and dynamics of multi-spike patterns for the one-dimensional Gray–Scott model. Eur. J. Appl. Math. **20**(2), 187–214 (2009)

Chossat, P., Iooss, G.: The Couette–Taylor problem. In: Mathematical Sciences, vol. 102. Springer, Berlin (1994)

Deblauwe, V., Barbier, N., Couteron, P., Lejeune, O., Bogaert, J.: The global biogeography of semi-arid periodic vegetation patterns. Glob. Ecol. Biogeogr. **17**(6), 715–723 (2008)

Devaney, R.L.: Reversible diffeomorphisms and flows. Trans. Am. Math. Soc. **218**, 89–113 (1976)

Doedel, E.J.: AUTO-07P: Continuation and bifurcation software for ordinary differential equations. http://cmvl.cs.concordia.ca/auto (2007)

Doelman, A., Kaper, T.J., Zegeling, P.: Pattern formation in the one-dimensional Gray–Scott model. Nonlinearity **10**, 523–563 (1997)

Doelman, A., Rademacher, J.D.M., van der Stelt, S.: Hopf dances near the tips of Busse balloons. Discrete Contin. Dyn. Syst. **5**(1), 61–92 (2012)

Eckhaus, W.: Asymptotic Analysis of Singular Perturbations. Studies in Mathematics and Its Applications, vol. 9. North-Holland, Amsterdam (1979)

Eckhaus, W., Iooss, G.: Strong selection or rejection of spatially periodic patterns in degenerate bifurcations. Physica D **39**, 124–146 (1989)

Elwell, H.A., Stocking, M.A.: Vegetal cover to estimate soil erosion hazard in Rhodesia. Geoderma **15**, 61–70 (1976)

Fowler, A.C.: Mathematical Models in the Applied Sciences. Cambridge Texts in Applied Mathematics. Cambridge University Press, Cambridge (1997)

Gardner, R.A.: On the structure of the spectra of periodic traveling waves. J. Math. Pures Appl. **72**, 415–439 (1993)

Gardner, R.A.: Spectral analysis of long wavelength periodic waves and applications. J. Reine Angew. Math. **491**, 149–181 (1997)

Gilad, E., von Hardenberg, J., Provenzale, A., Shachak, M., Meron, E.: Ecosystem engineers: from pattern formation to habitat creation. Phys. Rev. Lett. **93**(9), 098105 (2004)

Henry, D.: Geometric Theory of Semilinear Parabolic Equations. Lecture Notes in Mathematics, vol. 840. Springer, Berlin (1981)

HilleRisLambers, R., Rietkerk, M., van den Bosch, F., Prins, H.H.T., de Kroon, H.: Vegetation pattern formation in semi-arid grazing systems. Ecology **82**(1), 50–61 (2001)

Kato, H.: Quasi-linear equations of evolution, with applications to partial differential equations. In: Lecture Notes in Mathematics, vol. 448, pp. 25–70. Springer, Berlin (1975)

Kealy, B.J., Wollkind, D.J.: A nonlinear stability analysis of vegetative Turing pattern formation for an interaction–diffusion plant-surface water model system in an arid flat environment. Bull. Math. Biol. **74**, 803–833 (2012)

Kelly, R.D., Walker, B.H.: The effects of different forms of land use on the ecology of a semi-arid region in southeastern Rhodesia. J. Ecol. **64**, 553–576 (1976)

Klausmeier, C.A.: Regular and irregular patterns in semi-arid vegetation. Science **284**, 1826–1828 (1999)

van de Koppel, J., Rietkerk, M., van Langevelde, F., Kumar, L., Klausmeier, C.A., Frysell, J.M., Hearne, J.W., van Andel, J., de Ridder, N., Skidmore, A., Stroosnijdr, L., Prins, H.H.T.: Spatial heterogeneity and irreversible vegetation change in semiarid grazing systems. Am. Nat. **159**(2), 209–218 (2002)

Kéfi, S., Rietkerk, M., van Baalen, M., Loreau, M.: Local facilitation, bistability and transitions in arid ecosystems. Theor. Popul. Biol. **71**, 367–379 (2007a)

Kéfi, S., Rietkerk, M., Alados, C.L., Pueyo, Y., Papanastasis, V.P., ElAich, A., de Ruiter, P.C.: Spatial vegetation patterns and imminent desertification in Mediterranean arid ecosystems. Nature **449**, 213–217 (2007b)

Levefer, R., Lejeune, O.: On the origin of tiger bush. Bull. Math. Biol. **59**(2), 263–294 (1997)

Macfadyan, W.A.: Soil and vegetation in British Somaliland. Nature **165**, 121 (1950a)

Macfadyan, W.A.: Vegetation patterns in the semi-desert planes of British Somaliland. Geogr. J. **116**, 199–211 (1950b)

Matkowsky, B.J., Volpert, V.A.: Stability of plane wave solutions of complex Ginzburg–Landau equations. Q. Appl. Math. **51**, 265–281 (1993)

Mielke, A.: The Ginzburg–Landau equation in its role as modulation equation. In: Fiedler, B. (ed.) Handbook of Dynamical Systems, vol. II, pp. 759–835. Elsevier, Amsterdam (2002)

Morgan, D.S., Doelman, A., Kaper, T.J.: Stationary periodic patterns in the 1D Gray–Scott model. Methods Appl. Anal. **7**(1), 105–150 (2000)

Ni, W.-M.: Diffusion, cross-diffusion, and their spike-layer steady states. Not. Am. Math. Soc. **45**(1), 9–18 (1998)

Rademacher, J.D.M., Sandstede, B., Scheel, A.: Computing absolute and essential spectra using continuation. Physica D **229**(2), 166–183 (2007)

Rademacher, J.D.M., Scheel, A.: Instabilities of wave trains and Turing patterns in large domains. Int. J. Bifurc. Chaos Appl. Sci. Eng. **17**(8), 2679–2691 (2007)

Rietkerk, M., Ketner, P., Burger, J., Hoorens, B., Olff, H.: Multiscale soil and vegetation patchiness along a gradient of herbivore impact in a semi-arid grazing system in West Africa. Plant Ecol. **148**, 207–224 (2000)

Rietkerk, M., Boerlijst, M., van Langevelde, F., van de Koppel, H.H.T.J., Kumar, L., Prins, H.H.T., de Roos, A.M.: Self-organization of vegetation in arid ecosystems. Am. Nat. **160**(4), 524–530 (2002)

Rietkerk, M., Dekker, S.C., Wassen, M.J., Verkroost, A.W.M., Bierkens, M.F.P.: A putative mechanism for bog patterning. Am. Nat. **163**(5), 699–708 (2004)

Sandstede, B.: Stability of travelling waves. In: Fiedler, B. (ed.) Handbook of Dynamical Systems, vol. II, pp. 983–1055. Elsevier, Amsterdam (2002)

Satnoianu, R.A., Menzinger, M.: Non-Turing stationary patterns in flow-distributed oscillators with general diffusion and flow rates. Phys. Rev. E **62**(1), 113–119 (2000)

Satnoianu, R.A., Maini, P.K., Menzinger, M.: Parameter space analysis, pattern sensitivity and model comparison for Turing and stationary flow-distributed waves (FDS). Physica D **160**, 79–102 (2001)

Scheel, A.: Radially symmetric patterns of reaction–diffusion systems. Mem. Am. Math. Soc. **165** (2003)

Schneider, G.: Nonlinear diffusive stability of spatially periodic solutions—abstract theorem and higher space dimensions. Tohoku Math. Publ. **8**, 159–168 (1998)

Sherratt, J.A.: An analysis of vegetation stripe formation in semi-arid landscapes. J. Math. Biol. **51**, 183–197 (2005)

Sherratt, J.A., Lord, G.J.: Nonlinear dynamics and pattern bifurcations in a model for vegetation stripes in semi-arid environments. Theor. Popul. Biol. **71**, 1–11 (2007)

Sherratt, J.A.: Pattern solutions of the Klausmeier model for banded vegetation in semi-arid environments I. Nonlinearity **23**, 2657–2675 (2010)

Siero, E., Rademacher, J.D.M.: Stability of wavetrains in quasilinear parabolic systems on the real line (2012). In preparation

Thiery, J.M., D'Herbes, J.M., Valentin, C.: A model simulating the genesis of banded vegetation patterns in Niger. J. Ecol. **83**, 497–507 (1995)

White, P.L.: Brousse tigrée patterns in Southern Niger. J. Ecol. **58**, 549–553 (1970)